Development of sensors type LFIA for the detection and quantification of anti-toxoplasmosis antibodies

Leonardo Francisco Loureiro Ferreira
Master's degree in Applications in Biotechnology and Synthetic Biology
Chemistry and Biochemistry Department, Biology Department
2022/2023

Supervisor
Eulália Fernanda Alves de Carvalho Pereira, Associate Professor, Faculty of Sciences of University of Porto

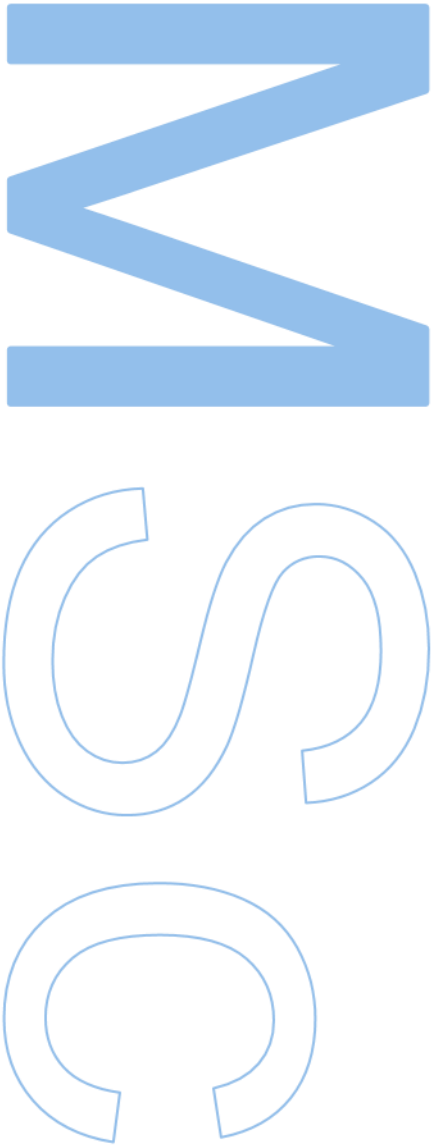


U.PORTO
FACULDADE DE CIÊNCIAS
UNIVERSIDADE DO PORTO

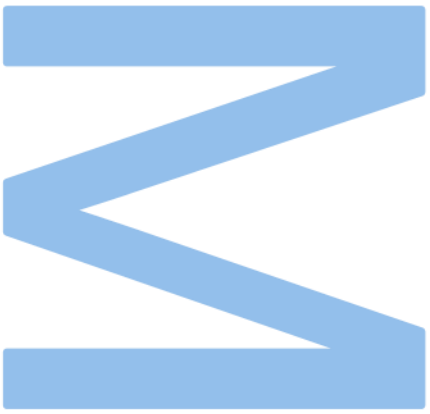

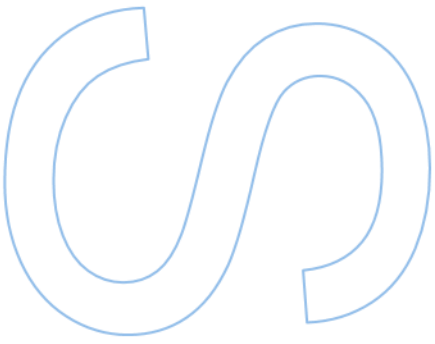

Dedicated to Professor Eulália Pereira and Doctor Maria Enea.

Acknowledgements

First of all, I'd like to thank 2 people that without which none of this would be possible, both literally and metaphorically, Professor Eulália Pereira and Doctor Maria Enea. Not a single day went by where I did not feel supported by both, whether that be in work, but also personally. Only by experience in life can some people understand what wisdom people before us tried to impart at us, and only after meeting these 2 great women I understood something once said by Sir Isaac Newton, "If I have seen further, it is by standing on the shoulders of giants". The person I am today and the work I present here were only possible due to their guidance, their unbound compassion and, the capacity to treat me not only as a person to teach, but also as a fellow human being and budding scientist. As such, I would never be able to ever repay them for everything they did for me, but though here I'd like them to know that during this year that I was with them they were not only inspirations but also my friends.

To my close group of friends, Pedro, Cátia, Rodrigo, Francisco and Ricardo. For always being there for me, for never giving up on me during my numerous and long rants, whether about work or about personal issues that plagued me, that they listened and supported me through thick and thin. As it is said "The blood from the covenant is thicker than the water from the womb", and such I only want to say that you proved once and once again that you are not only my friends, but also my family. For everything we passed together, our bond is stronger that diamonds and as unbendable as mercury.

To my sister for always being there to comfort me and help me when needed, and in pair with my little nephew/god-son gave me power to continue my work, so that they may look proudly on me.

And finally last but never least my closest friend and the one that most had to tolerate me during this year, my best friend Inês Monteiro, you were always there for me, never doubted me even when I started to doubt myself. No words serve to describe you and all you and all you ever did for me. Therefore, I would just like to say this for you, thank you for all you ever did for me and will ever due, and always remember that you will always be the other part of my soul, for as the ancient Greeks certainly knew, we had to be separated for even the gods would fear us together.

Resumo

A toxoplasmose é uma doença causada por infeção do protozoário *Toxoplasma gondii,* normalmente assintomática e não-letal. Contudo, é perigosa para indivíduos imunossuprimidos e fetos. Os casos de infeção congenital podem levar à morte do feto. É assim necessário detetar a presença de infeção o mais precocemente possível. Os testes atualmente disponíveis são demorados, exigem pessoal altamente qualificado e são caros. A nanotecnologia tem mostrado um elevado potencial para resolver estes problemas em biossensores. Em particular, os bionanossensores baseados em nanopartículas plasmónicas de ouro têm demonstrado ser uma alternativa fiável em imuno-ensaios. Neste trabalho, utilizaram-se nanopartículas de ouro para desenvolver um ensaio simples e fiável para detetar a presença de anticorpos contra *Toxoplasma gondii*. Prepararam-se nanopartículas de ouro e modificaram-se com um péptido sintético, que tinha demonstrado anteriormente uma forte ligação a anticorpos contra *Toxoplasma gondii.* Os bionanoconjugados preparados foram caracterizados por espetroscopia de visível, Espalhamento de luz dinâmico (DLS) e Análise por Rastreamento de Nanopartículas (NTA). Os resultados obtidos mostram que os bionanoconjugados apresentam uma boa estabilidade coloidal e que poderão ser utilizados como sondas para deteção por espectroscopia de visível ou por espetroscopia Raman Aumentada pela Superfície

Palavras-chave: Toxoplasmose, nanotecnologia, SERS, nanopartículas de ouro, nanoestrelas.

Abstract

Toxoplasmosis is a disease caused by infection with the protozoan *Toxoplasma gondii*. The disease normally is asymptomatic and non-lethal. However, it is dangerous for immunosuppressed individuals and unborn foetus. In cases of congenital infections, it may lead to death of the foetus. It is thus critical to detect the presence of infection as early as possible. Currently available tests are time-consuming, require specialized techniques and are expensive. Nanotechnology has shown great potential to overcome these problems in bio-sensing. In particular, bionanosensors using the plasmonic particles of gold nanoparticles proved to be a reliable alternative in immuno-essays. In this work, we have used gold nanoparticles to develop a simple and reliable test to detect the presence of antibodies against *Toxoplasma gondii*. Gold nanoparticles were prepared and modified with a synthetic peptide, that has previously shown to strongly bind to antibodies against *Toxoplasma gondii.* The bionanoconjugates prepared were characterized by visible spectroscopy, Dynamic Light Scattering and Nanoparticle Tracking Analysis. The results obtained show that the bionanoconjugates present a good colloidal stability, and can be further used as probes for detection by visible spectroscopy and Surface Enhanced Raman Spectroscopy.

Keywords: Toxoplasmosis, nanotechnology, SERS, gold nanoparticles, nanostars.

Table of Contents

List of Tables

List of Figures

List of Abbreviations

AuNP	GOLD NANOPARTICLES
AuNS	GOLD NANOSTARS
Tri-sodium citrate	TRISODIUM CITRATE DI-HYDRATE
PEG	2-(2-[2-(11-MERCAPTO-UNDECYLOXY)-ETHOXY]-ETHOXY)-ETHOXY-ACETIC ACID
AuNP-PEG	PEGYLATED GOLD NANOSPHERES
AuNS-PEG	PEGYLATED GOLD NANOSTARS
EDC	1-ETHYL-3-[3-(DIMETHYLAMINO)PROPYL]CARBODIIMIDE
NHS	N-HYDROXYSUCCIMIMIDE
AuNP-PEG-GRA6II	PEGYLATED GOLD NANOSPHERES FUCNTIONALIZED WITH GRA6II SYNTHETIC PEPTIDE VIA EDC/NHS CHEMISTRY
AuNS-PEG-GRA6II	PEGYLATED GOLD NANOSTARS FUCNTIONALIZED WITH GRA6II SYNTHETIC PEPTIDE VIA EDC/NHS CHEMISTRY
IGG	IMMUNOGLOBULIN G
IGM	IMMUNOGLOBULIN M
LFIA	LATERAL FLOW IMMUNOASSAY

Introduction

Toxoplasmosis – a protozoan threat to the unborn

Toxoplasmosis is a disease caused by infection by Toxoplasma gondii, an ubiquitous, facultatively heteroxenous, polyxenous protozoon that has evolved to develop several routes of dissemination within and between a panoply of hosts [1-4]. T. gondii has the capacity to infect nucleated cells of nearly all warm-blooded animals. Human infection via the T. gondii protozoon presents several possible routes such as : I) ingestion of infectious oocysts present in the environment (such as ingestion of food or water contaminated with feline faecal matter or interaction with soil or other contaminated materials such as litter boxes); II) ingestion of tachyzoites contained in animal products such as meat, primary offal, and blood from contaminated animals, tissue transplants and even unpasteurized milk; and III) vertical dissemination from mother to foetus via the placenta [1, 2, 5, 6].

Toxoplasma gondii infection in humans is usually asymptomatic and non-threatening to human beings due to the potential hosts innate immune system resisting the pathogens proliferation. However, in certain groups of people, such as in immunocompromised individuals, pacients under treatment with immunosuppressors or chemotherapy, and pregnant women, T. gondii is an opportunist pathogen [5, 7, 8]. Risks of developing encephalitis, myocarditis or pneumonitis is frequent in immunocompromised and cancer patients undergoing chemotherapy[8]; and in cases of infection during pregnancy, congenital infection with *T. gondii* have proven capable of provoking ocular damage [3, 4], which in some cases may even lead to severe sight damage or even total blindness, hydrocephalus and stillbirth in foetus [2, 7, 9, 10]. The infection path in pregnancy is shown in figure 1.

Thus, monitorization of toxoplasmosis infection during pregnancy is critical, since failure to do so can be lethal [2, 8, 9, 11-13]. The essays used nowadays for the detection of the protozoan originated disease include serological essays, essays for the detection of *Toxoplasma*-specific antibodies, such as Enzyme-linked Immunosorbent Assay (ELISA)[14-19], or biological biopsy by histological identification of the parasites [20]. However, such essays are time-consuming, require highly-qualified personnel, and expensive. In addition, these essays are prone to false positive results due to the way the immune system deals with the infection [21-23].

In acute infection, immunoglobulin G (IgG) is produced by the immune system and it can be detected as early as three days post-infection, serving as a marker for detection of acute infection. [15, 24-27]. After, the production of immunoglobulin M (IgM) begins, providing a long-term immune response. Due to such long-term immune by IgM response it becomes possible to distinguish an acute case of Toxoplasmosis and a case of a prior case of infection. In cases of acute infection both presence of IgG and IgM can be detected by immunoassays, however if only IgM can be detected by the same tests that means that infection has been established in a previous time, sometimes going as further as months or even years. It is in the case of acute infections during pregnancy that the disease can be dangerous to the unborn infant [28]. Infection prior to pregnancy is not dangerous to the foetus. Many of the current immuno-essays for the detection of infection via *T. gondii* are too wide in detection spectre, and are sensitive to IgM remaining in the hosts system, leading to the occurrence of false positives[25]. However, no guidelines for detection and reporting of *T. gondii* acute infections in pregnancy or immunosuppression exist, making the control and treatment of the cases difficult [29-31].

As such, the necessity of cheap and efficient tests, which in parallel present a fast response rate to the possibility of infection is on the rise. These would be a valuable tool to specifically detect cases that may be harmful for patients, whether unborn or not, so that faster and improved responses to such cases may be done. Amongst immunosuppressed cases and congenital cases, congenital cases are harder to detect since the mother presents no symptoms whatsoever, only the foetus being impacted.

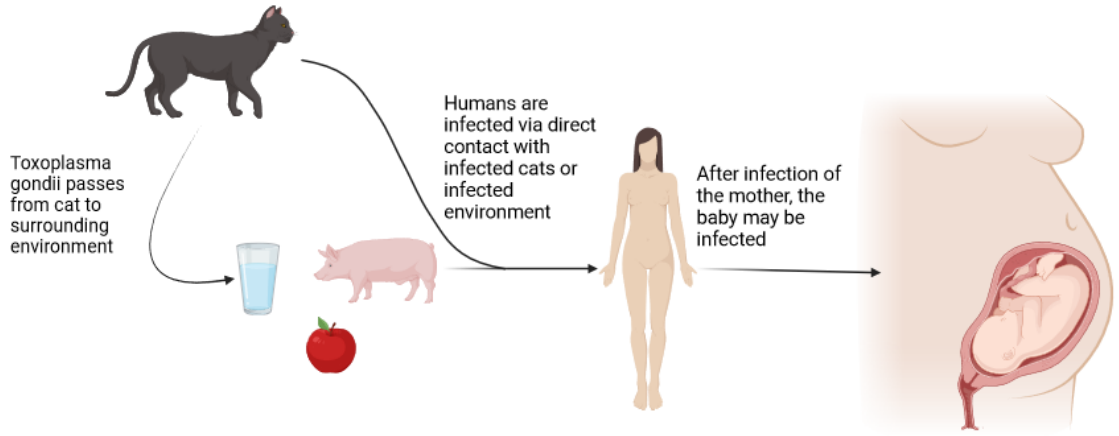

Figure 1 – Visual schematization of the simplified method of infection of *Toxoplasma gondii* from an infected cat (the protozoan primary host) to the pregnant mother and the unborn foetus (secondary hosts).

Therefore, a test catered for the use in possible infection in pregnancy is of the highest priority.

Nanoparticles – Paul Ehrlich's legendary magic bullet?

Paul Ehrlich, winner of the 1908 Nobel Prize in medicine, in conjunction with Elie Metchnikoff, on his work in the field of Immunology, of which he is still considered by a great number of scientists one of the big pillars and fathers of, once had created an idea of a magical, yet simply scientifical, particle capable of healing almost every disease without repercussion, which he baptised as the "magic bullet"[32, 33]. Dr Ehrlich, amongst many other hypothesis and ideas, created the *Therapia Magna Sterilizans*, also known by many the "magic bullet", which envisioned the use of a specific chemical substance that presented high affinity for pathogens and toxins in the human body, being able to treat the affected patients in doses high enough to treat them of their malady, but in concentrations low enough to be harmless to the patient [32-34].

Nanotechnology borrows a lot from this concept, allowing to create systems that respond with incredible affinity to certain triggers, such as the presence of a pathogen or parts of it, and even non-infectious diseases such as cancer[35]. Upon detection of such triggers it may have a panoply of effects based on what it was specifically created for, being able to detect the diseases in cases of elaborations of sensors, or even release previously loaded drugs that are released upon certain stimuli characteristic to the malady being treated[27, 36-45]. As such, nanotechnology allows for a completely local treatment of the disease, allowing for an extreme reduction of such drug in other places and organs in the human body, where they could be harmful.

As such, from a certain point of view, Paul Ehrlich can be considered as one of the fathers of nanomedicine, not for work he elaborated in the field, but because of this idea, and is highly associated with the field. As many people in the scientifical field know, all great theories and laws discovered started by a single idea, sometimes and idea that may have at its time be considered an impossible, impossibly idyllic, or even

crazy one. A single idea from a great mind is giving rise to numerous works of great value, for as the writer and poet Gioconda Belli once said “The world has always gone forward when people have dared to have crazy ideas.”

Nanotechnology, not being the perfect magic bullet, allows for the preparation of nanoparticles and nanosystems with great promise and compatibility for usage in many types of scientific work, and they are extremely promising in the medical, biological, and biomedical fields, that times past could only be dreamed of in terms of combined efficiency, cost-efficiency, portability and even user interface for facility of use by medical and even common people to use easily and competently. However, it becomes necessary to understand why and how nanoparticles work.

Nanoparticles, the fundamental component of nanotechnology, are particles with at least one dimension within 1 to 100 nanometers and may be made by a panoply of materials[34, 35]. Due to their reduced size, which allows for a larger surface area to volume ratio, and to their increased reactivity in chemical processes, amongst many other properties, nanoparticles exhibit a panoply of inherent chemical, physical and biological properties when compared with larger nanoparticles[46]. As for the materials that may be used in the synthesis of nanoparticles they may be distinguished and separated in 2 groups (Figure 2): I) organic nanoparticles, which synthesis basis are organic compounds such as proteins or lipids; this group normally presents high degradability and low toxicity, and are normally used as efficient drug vehicle systems to biological systems in biomedical areas[35, 47]; II) inorganic nanoparticles, which are normally created using as a basis metals[48] or metal oxides[49], or carbon[50]; such group normally present smaller sizes, and characteristics such as crystalline and amorphous structures, easily changeable morphologies, as shown in figure 3, to obtain better sensitivity and reactivity to certain environmental factors such as heat and electromagnetic radiation amongst many others[35].

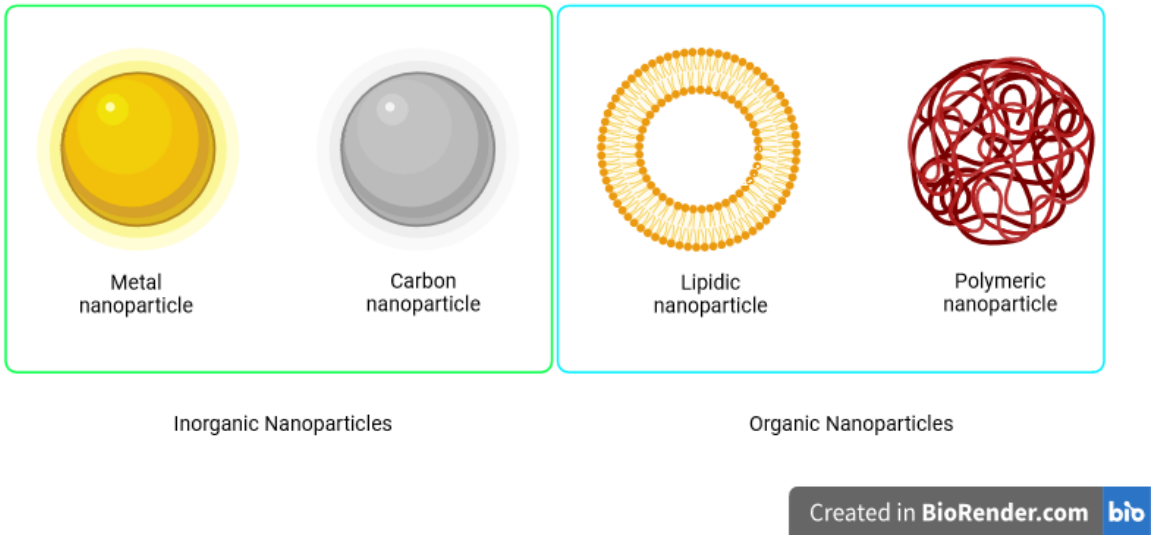

Figure 2 – Visual representation of the different groups of materials that can be used as a basis for nanoparticle synthesis. Some characteristics such as surface morphology of nanoparticles may be seen.

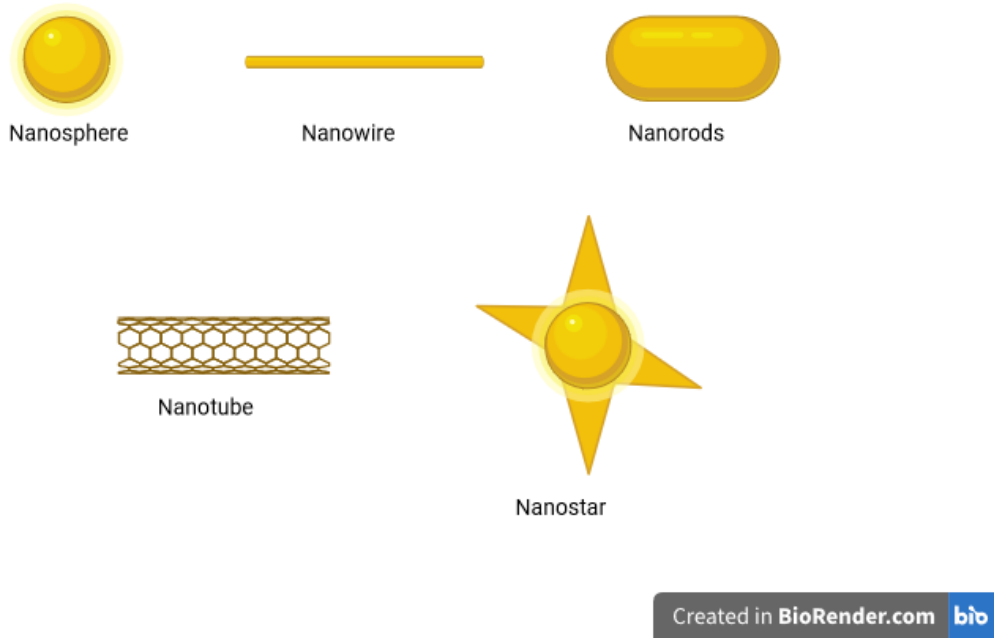

Figure 3 – Visual representation of the different morphologies that nanoparticles may present. The morphologies shown are shapes normally utilized in works using as a basis noble metal, such as in the present work.

In order to obtain nanoparticles, there are many methods of synthesis described in the literature; however, they can be all distributed between 2 groups of synthetic methods[35]: Top-down Methods[48, 51, 52], or Bottom-up Methods[53, 54] (Figure 4).

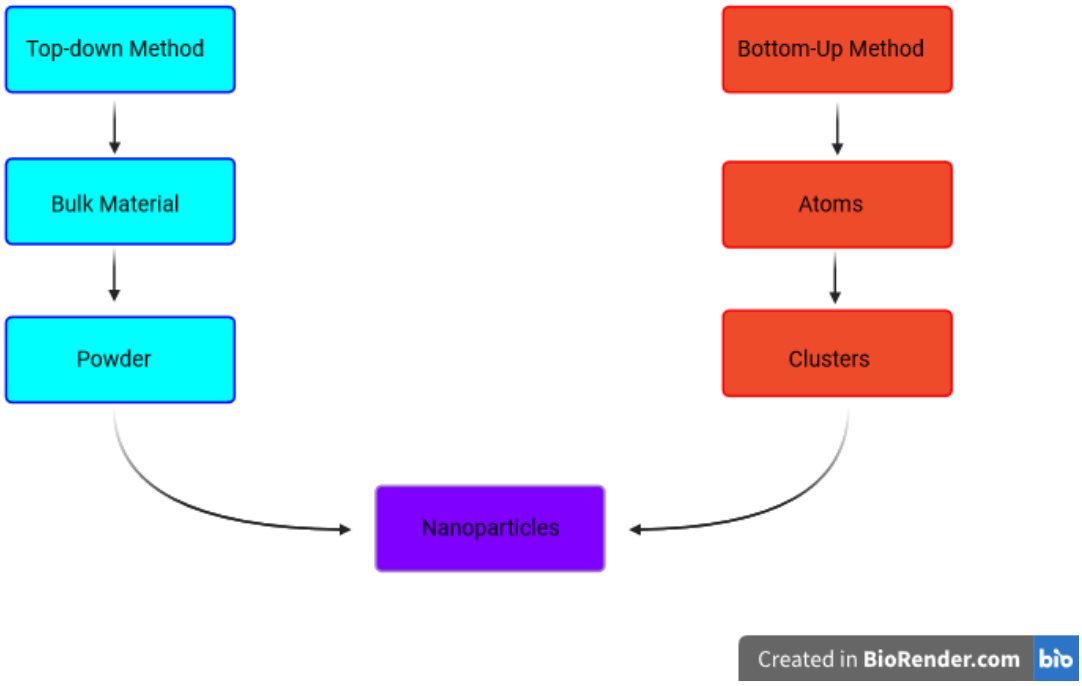

Figure 4 – Visual representation of the different groups of synthesis methods for the creation of nanoparticles.

In the cases were top-down methods (also known as destructive methods) are used, a bulk material of relative high volume is reduced until the desired nanometric scale is obtained. Some examples of the most common top-down methods are nanolithography[52, 55], sputtering[56, 57], laser ablation[58], thermal decomposition[48], and mechanical milling[51].

Conversely, bottom-up methods (also known as constructive methods) are based on the growth of the nanomaterials from their atomic or molecular units to obtain the desired size and morphology of nanoparticles. Examples of most commonly used bottom-up methods are pyrolysis[59, 60], biosynthesis[61], sol-gel[53], spinning[54], and chemical vapour deposition[50].

After nanoparticle synthesis, the obtained particles should be carefully characterized as soon as possible and regularly, this due to the high potential of post-

synthesis modification of the nanoparticles surface, such as surface functionalization and surface charge alteration[35]. Surface charge of nanoparticles normally presents itself as positive, negative, or zwitterionic, surface charge alters parameters such as nanoparticle-target interaction, dispersion amongst the nanoparticles via same-charge repulsion effects, and solution stability[35]. The surface of the nanoparticles may also be functionalized with a series of materials such as peptides, desoxyribonucleic acid (DNA), ribonucleic acid (RNA), antibodies, lipids, intermediary linker group and many more types of molecules[14, 18, 42, 62, 63]. Normally, such functionalization serves a purpose specifically tailored for the application. As an example, PEG is normally used when the synthesized nanoparticles are to be used in physiological and biological media, such as for *in vivo* injection for disease treatment[64-67]. This is due to the stealthing properties of this molecule, so the nanoparticles introduced in the biological system are not as easily detected by the immunological system of the receiver of the nanoparticle injection, and as a stabilizing agent that minimizes non-desirable binding[68-73]; in another example DNA, RNA and antibodies are utilized for the detection of specific diseases or genes, such as the identification of carcinogenic genes or parasite induced diseases[17, 67, 74-78].

Nanoparticles and toxoplasmosis – Is the creation of a mass immunoassay test for the detection of congenital toxoplasmosis possible?

Utilizing the knowledge presented in chapter “Nanoparticles – Paul Ehrlich’s legendary magic bullet?” of the introduction, the question arises: could nanotechnology be utilized for the creation of a test that allows for an easy and inexpensive, yet effective detection of the parasite induced malady?

To answer such question another must be answered first: since nanoparticles need a target to be detected or directed onto for tailored functionalization, does toxoplasmosis possess such target for detection? The answer is yes. During infection a series of peptides, with extremely variable functions are synthesized by the protozoan to allow its proliferation and survival, and one in specific, the Gra6II peptide[14, 15, 17, 18, 79], which is a peptide that presents host infection properties, not only has been well studied in other works[79] Gra6II is derived from the Gra6 protein C-terminal end, and presents target epitopes to which, as observed in other studies, the antibodies synthesized by the hosts immune system bind to in a specific and sensitive way[15, 18,

79-82]. When an antibody detects the parasitic peptide, it does not detect the entirety of the peptide chain, it detects solely segments of such protein, which are called epitopes; the epitopes connect to a specific part of the antibodies, located in the terminal zone of the variable fragments of the antibodies, such binding zone is denominated as paratope[83-86] (figure 5).

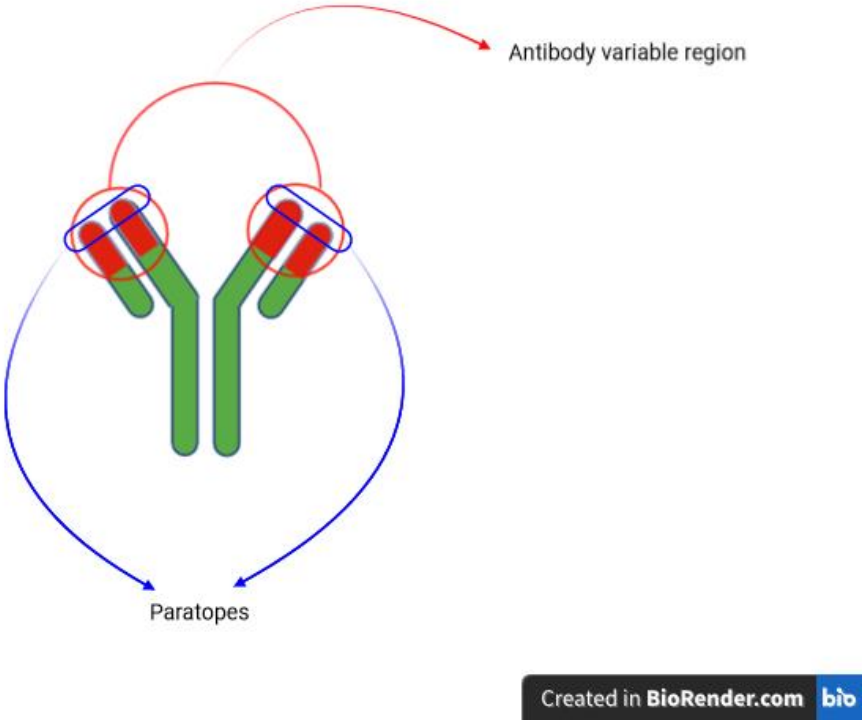

Figure 5 – Visual representation of an antibody, in specific and IgG. The antibody variable regions and the paratopes located at the terminus at the same have been identified.

Therefore, when one of such sequences that functions as an epitope could be affixed onto nanoparticles, the antibodies would be able to bind to the nanoparticles as if it were a case of infection, leading to a binding of paratope to epitope, such as has been observed in a high number of other studies. With the appropriate nanoparticle material as a basis that presents a specific group of characteristics to be used as a detecting immunoassay, even more functionalities can be added. One group that exhibits tremendous potential are inorganic nanoparticles, such as noble metals. Specifically gold nanoparticles have been presented in literature as the ideal material for such studies[36, 37, 43, 87-95]. Gold nanoparticles show great potential due to its

interaction to visible light, which allows for the facilitations of usage of the immunoassay via the target user, and for a more accentuated quickness in obtaining results [37, 88-90, 93, 94, 96-100].

Gold nanoparticles can be functionalized with a Gra6II epitope, and used to detect the presence of anti-toxoplasmosis antibodies, such as immunoglobulin G (IgG) in cases of recent ongoing infection, or immunoglobulin M (IgM) in cases of infection at an earlier time frame. Work formerly made in this laboratory showed the great promise of the functionalization of nanoparticles with Gra6II epitopes for the detection of anti-toxoplasmosis antibodies[77]. The basis of the test would be that upon the binding of epitope-paratope, a high avidity could be verified, meaning that the same antibody doesn't necessarily connect to a sole nanoparticle, being totally possible for the connection of a sole antibody to 2 peptide functionalized nanoparticle[77]. As such, when in contact with *T. gondii* host infected serum an alteration in properties can be detected, in this case due to changes in colour of the nanoparticles. Such colour variation is attributed to the aggregation of the nanoparticles, which in turn alter the wavelength at which the attenuance peak appears. Such tests that rely in the nanoprobes aggregations to obtain results are normally denominated as "sandwich tests"[101-104] (Figure 6). Addition of salt to the test is a common practice to allow for an increase in effectiveness of the process. Upon all this, the production of gold nanoprobes functionalized with toxoplasmosis epitope peptides for the detection of toxoplasmosis via detection of anti-toxoplasmosis antibodies binding seems likely to present great potential for the detection of the potentially fatal cases of congenital toxoplasmosis, such as the work done by Sousa et al. [77]. Although, would the possibility of using a different shape, such as nanostars due to such shape being known for great potential in Surface-Enhanced Raman Scattering (SERS) tests, lead to an improved and easier manufacturing process, utilization by non-specific personnel and better overall satisfaction with the final product?

SERS tests present themselves as a great method of detection of biological molecules, being those peptides[62, 67, 76, 105], antibodies[35, 36, 38, 39, 106, 107], DNA or RNA strands[14, 42, 63, 108], amongst many others. SERS tests which utilize noble nanoparticles as a basis for detection presents identification of targets analytes, without to the need to utilize complex chemistry techniques, time-consuming-steps or the utilization of fluorescent label molecules, while rivalling the sensitivity of other fluorescence-based detection techniques[37, 109, 110].

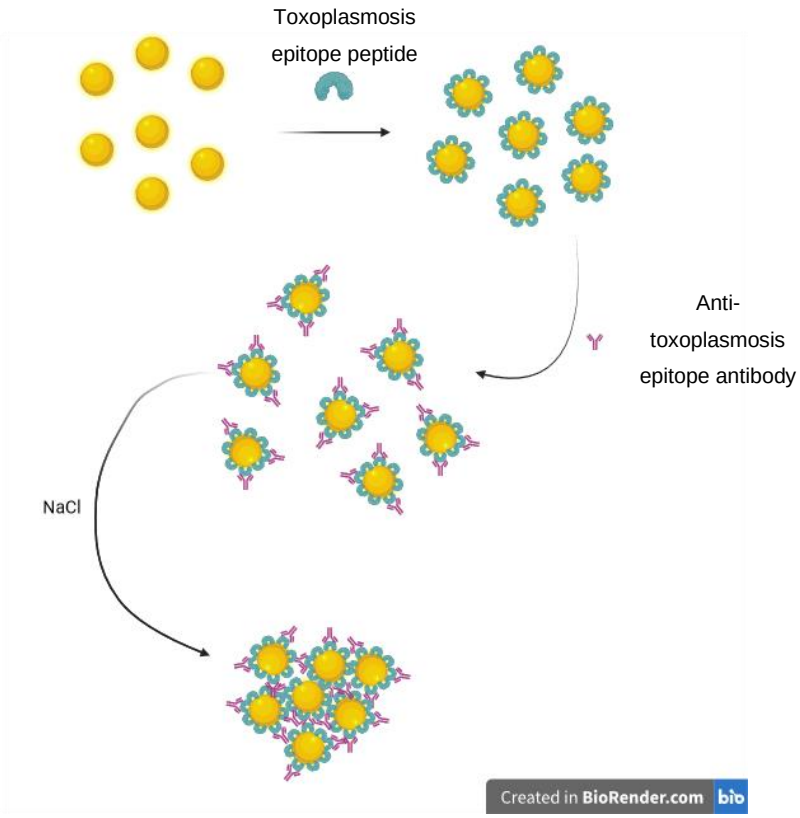

Figure 6 – Visual representation of a sandwich test immunoassay utilizing as a basis toxoplasmosis epitope peptide functionalized gold nanoparticles for the detection of anti-toxoplasmosis antibodies. Upon the addition of salt and infected serum (from which the anti-toxoplasmosis antibodies is localized) particles will aggregate and the sandwich test will be completed

Morphologically, the main difference between nanospheres and nanostars is the presence of sharp branches that are formed from the spherical gold core. Such modifications allow for the nanostars to be ideal contenders for application in SERS immunoassays[37, 89, 90, 93, 100]. The presence of such branches allows for the creation of “hot spots”, which confers an enhancement of the electromagnetic field (EM) of the nanoparticles, which in turn leads to an enhancement to the nanoparticles plasmonic field when compared to nanospheres[111-114]. Plasmonic field refers to focalized oscillations of electron density related to fixed positive ions in the metallic nanoparticles (Figure 7), different plasmonic fields lead to different plasmon band. Plasmon band, also referred to as surface plasmon resonance (SPR), refers to the capacity of the particle to absorb and scatter energy from light sources, especially at certain wavelengths of the light spectrum, whether it be from lasers or even from light sources as solar energy. When specific wavelengths of radiation are introduced to the nanoparticles an electronic excitation occurs, absorbing and scattering light at a much higher efficiency than identical sized and morphologically non-plasmonic particles[109].

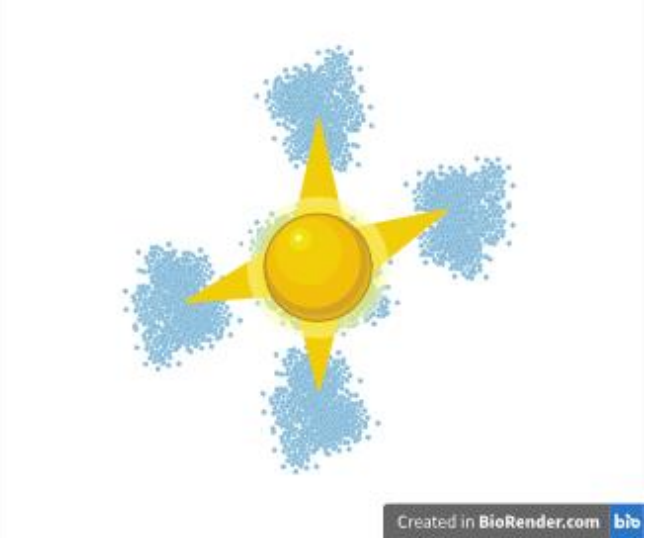

Figure 7 – Visual representation of the 2 points of EM focalization (presented in blue). The anisotropic nanostars (presented in yellow) present a high intensity EM focalization in the tips of the branches and a low intensity EM focalization in the metallic core of the nanoparticle.

When utilized in immunoassays, SERS type tests normally are incorporated in microfluidic systems, such as Lateral Flow Immunoassays (LFIAs) [115-118]. LFIAs are easy to use and cheap point of care systems that allow for the creation of a robust, rapid in results obtainment, specific and sensitive to the target molecules, while still being user-friendly and specific result development equipment free. Such tests when combined with the SERS capabilities of gold nanoparticles, present a much quicker response than normally utilized tools for toxoplasmosis identification, needing only a few minutes for result obtainment while at the same time being a single step technique[119-121].

The LFIA test would work by the introduction of a solution were the serum of the patient is contained in a specific orifice, after that the solution would permeate into the membrane and over time diffuse over it. At a certain point the solution would enter in contact with the created nanoprobes bond to the membrane of the LFIA microfluidics test. Then in the “sandwich test”, also known as direct assays, the analyte, in this work it being the anti-toxoplamosis antibodies, would react with the epitope of the synthetic Gra6II peptide epitope bond to the nanoparticles, leading to an aggregation of nanoprobes[122, 123]. Such aggregation would lead to either a visual change of colour of the bar would signify a positive result, i.e. a case of infection, while if the colour of the bar remained unaltered the test would be negative, i.e. no infection evidence is observed[77]. This type of test allows also for the use of concomitant detection bands,

and as explained before, the quantification of IgG and IgM and their comparation allows for the clarification in case of infection[24, 26, 27, 38, 40, 124]. If infection is of an acute nature, the presence of both IgG and IgM at the same time, i.e. two positive results, would be verifies, and therefore dangerous for the unborn child; however, if only the IgM band presents itself as positive it would mean that the infection is not of an acute nature, and therefore not dangerous for the unborn. If both bands do not present any change, i.e. are both positive, there is and never was an infection of *T. gondii* for the patient in question.

In this work, the possibility of utilization of gold nanospheres and gold nanostars as nanoprobes in LFIA sensors for the detection and quantification of anti-toxoplasmosis antibodies is analysed and compared.

Materials and Methods

Materials

The following reagents were used: gold (III) chloride solution, 30 % wt. Au in dilute hydrochloric acid (HCl), from Sigma-Aldrich, Portugal: tri-sodium citrate di-hydrate PA-ACS, >99%, from Panreac Applichem, Germany; silver nitrate, 99.9999%; Sigma-Aldrich, Portugal; L-ascorbic acid, TraceSELECT®, ≥99.9998%; Fluka Analytical (Portugal); hydrochloric acid 37%, Fisher Chemical, Loughborough, UK; nitric acid 65% for analysis, ISO; Panreac Applichem, Germany; potassium phosphate dibasic ACS reagent, ≥98%; Sigma-Aldrich, Portugal; potassium phosphate monobasic ACS reagent, ≥99%; Sigma-Aldrich, Portugal; 2-(2-[2-(11-mercapto-undecyloxy)-ethoxy]-ethoxy)-ethoxy-acetic acid (PEG ($HS-(CH_2)_{11}EG_3OCH_2-COOH$)), >95%, Prochimia Surfaces Sp. Z.o.o., Poland; 1-ethyl-3-[3-(dimethylamino)propyl]carbodiimide (EDC), BRAND, N-Hydroxysuccimimide (NHS), BRAND; GRA6 II antibody (peptide sequence: LHPGSVNEFDF), >95%, Caslo ApS, Denmark.

All chemicals and reagents were of the highest purity available. Ultrapure water (18.2 MΩ ・cm at 25 °C, Milli-Q®) was used to preparate all solutions, unless stated otherwise.

Synthesis of 15 nm gold nanospheres

All glassware was treated with aqua regia to remove metal residues. Aqua regia is a strong acid created from a ratio of 3:1 of hydrochloric acid:nitric acid (nitric acid should always be added to the nitric acid and never the other way around); aqua regia presents a high risk to the user if inhaled, ingested or having direct contact with due to its high corrosivity; safety guides should always be accessed before any handling of aqua regia and appropriate personal protective equipment such as a lab coat, protective eyewear, neoprene or butyl gloves, protective mask and neoprene apron should be used in use to guarantee personal safety [125]. After the aqua regia wash, the glassware was thoroughly washed with deionized water and, finally with ultrapure water (18.2 MΩ ·cm at 25 °C, Milli-Q).

Fifteen nm Gold nanospheres (AuNPs) were synthesized by the Turkevich-Frens method[126-128]. 0.2020 g of trisodium citrate di-hydrate was dissolved in 100 mL of

ultrapure water in a 250 mL Erlenmeyer and brought to reflux. 69.2 mL of gold (III) Chloride solution (HAuCl4) was added to the solution stirred at 1150 rpm. Immediately after the addition of HAuCl4, stirring was reduced to 700 rpm. After 5 minutes, the heating was turned off and the solution was left to cool to room temperature. The resulting suspension was stored at 4 °C.

Synthesis of 50 nm gold nanospheres

For synthesis of gold nanoparticles (AuNP), firstly a citrate solution (2.2 mM) was prepared via dissolution of 0.0971 g of trisodium citrate 2-hydrate in 150 mL of ultra-pure water. The citrate solution was then put under stirring of 750 rpm, and heated in a paraffin oil bath until the solution reached 100ºC. The system was fitted with a condenser with running water, a flask cap, and a cap/adaptor with a thermometer.

Once the temperature was reached, 1mL of a 25 mM HAuCl4 was added and left under stirring and boiling under the same conditions for 10 minutes. The HAuCl4 was made via dilution of 86.5 mL of HAuCl4 stock solution. After 10 minutes have come to pass the solution should now have a pink/ruby red tone, and the solution is cooled down until it reaches 90ºC, having now been obtained nuclei/seeds for growth of nanoparticles.

To proceed with the synthesis, upon the solution reaching 90ºC and having the temperature reaching stability; 2 more additions of 25 mM HAuCl4 solution were made, and after each addition 30 minutes resting synthesis time under heat and stirring is needed. At this point, 55 mL of sample is to be removed and 53 mL of ultra-pure water and 2mL of a 60 mM sodium citrate solution was added. Again, 2 extra additions of 1 mL of 25 mM HAuCl4 with 30 minutes resting time under stirring and heating were made.

Upon all steps being concluded, the solution was left to cool down to room temperature. Once cooled down the solution was transferred into a storage flask and left to rest overnight. Whenever not in use the solution was stored in the fridge at 4ºC.

Gold Nanostars Synthesis

To synthesize gold nanostars, ultra-pure water was added to and Erlenmeyer and placed under stirring of 900 rpm, in a cold bath of temperature between 1 to 3° C. Then, quickly yet carefully all reagents were added to the centre of solution, following an order of 1.445 M of HAuCl4, previously synthetized AuNP solution, and finally a simultaneous addition of 200 mM ascorbic acid and 8 mM silver nitrate. Both the solution of ascorbic acid and silver nitrate were made fresh immediately before the addition of such reactants, and before the simultaneously addition of ascorbic acid and silver nitrate the stirring was increased to maximum. When all reagents were added, the stirring speed was set to 900 rpm and left to react for 5 minutes. All volumes of the reactants were calculated considering the concentration of the gold nanostars utilized as seeds, the concentrations of the reactants used and a final concentration of nanostars of 0.17 nm.

Gold nanospheres and gold nanostars characterization

Visible spectra were obtained in a UV-Vis spectrophotometer GENESYS 10S UV-Vis, Thermo Scientific, using optical glass cells, with 1 cm optic pass (Hellma), at room temperature. AuNPs were diluted 4 times with ultra-pure water, while for AuNS a dilution factor of 5 was used for characterization of non-functionalized and PEGylated nanoparticles; for AuNP-PEG-Gra6II and AuNP-PEG-Gra6II a dilution of 150 μL of nanoparticle solution was diluted in 850 μL of ultra-pure water. When characterizing nanoparticles specific parameters were used: the scan started at 200 nm of wavelength and ended at 1000 nm of wavelength, attenuance value was used as measurement mode, for the vertical axis a value of 0 and 1 were respectively used for the minimum vale and maximum value, finally threshold of 0.01 value of attenuance and a peak pick was set for the maximum of each peak. Calculations for the determination of diameter and concentration of the spherical nanoparticles were based on the relations based by Haiss et al. [129].

Dynamic light scattering (DLS) and electrophoretic light scattering (ELS) measurements were performed in a Zetasizer Nano Series Nano – ZS; Malvern Instruments. using disposable cells (Malvern DTS1070). For DLS measurements the equipment presented a laser angle of 173° Backscatter (NIBS default), with a general-purpose analysis model. For each sample 5 measurements of 11 runs each were

made. For ELS measurements the equipment presented an 12.8° angle between the scattering beam and laser beam that passes through the centre of the sample, the Smoluchowski approximation model was utilized for the calculations via Henry calculations. For each sample 5 measurements were made, presenting them a number of runs between a minimum of 10 runs and maximum of 100 runs. Dilutions were the same as used in UV-Vis characterization.

NTA (Malvern NTA Nanosight NS300) was in suspensions obtained by diluting the suspension of non-functionallized nanostars or PEGylated nanostars 100-200 times and 50-100 times for non-functionalized nanospheres and PEGylated nanospheres. The dilutions used for Gra6II conjugated nanospheres and Gra6II conjugated nanostars were the same dilution: a dilution of 50 μL of nanoparticle solution was diluted in 950 μL of ultra-pure water. For signal acquisition the equipment's camera value was set to a level of 10 and screen gain to a value of 10, 5 repetitions of data of 60 seconds each were taken for qualitative analysis, all measurements were made at 25° C and when complete exported.

PEG Functionalization

PEG functionalization of the nanoparticles was made by incubation of 5 mL of the suspension with 0.300 mol/L PEG ($HS\text{-}(CH_2)_{11}EG_3OCH_2COOH$) in ratios 1:500 to 1:57800), for 1 hour, under stirring at 300 RPM. A functionalization control, in which no PEG was added was also made. After incubation, the samples were washed one time by centrifugation (mini spin, MiniSpin® series), for 10 minutes, at 2500 g and resuspension in 2mL Phosphate Buffer 2 mM, pH 7. Controls were subjected to the same procedure, but they were resuspended in 2 mL of ultra-pure water. All samples were stored at 4 °C.

Gra6II Functionalization

Gra6II synthetic peptide functionalization of the PEG functionalized nanoparticles was made via creation of a medium solution of nanoparticles + Phosphate Buffer pH 7 2mM (to the point that final concentration of nanoparticles would be equal to 0.2 nM was achieved). That same Nanoparticle/buffer medium was put in ice and addition of EDC at a concentration of 1 mM and of NHS at a concentration of 1mM was made,

following a ratio of 1:2 of EDC:NHS. Following such addition, the mixture was removed from ice and put under incubation for 15 minutes at approximately 300 RPM. After incubation, the samples were washed by one centrifugation (mini spin, MiniSpin® series), for 10 minutes at 2500 g for nanospheres and approximately 1300 g for nanostars, and resuspension was made via removing the supernatant and redispersing the pellet in phosphate buffer pH8 2mM, until half of final volume is attained.

Gra6 II:Nanoparticles ratios of 1000; 5000; 7500; 10000; 25000 and 50000 were created via addition of previously calculated volumes of Gra6II to the solutions created post centrifugation. Such calculations were made based on the concentration of nanoparticles in solution and the concentrations of Gra6 II available (in this work the concentrations used were of 0.396 mM and 0.0396 mM). After the peptide addition, the solution was let to incubate with a mixture of the nanoparticle solution previously obtained, ultrapure water, phosphate buffer pH7 2 mM and the Gra6 II peptide, for 2 hours under an agitation of approximately 450 RPM. After incubation the solution of each eppendorfs was washed by one centrifugation (mini spin, MiniSpin® series), for 10 minutes at 2500 g for nanospheres and approximately 1300 g for nanostars, followed by a removing of the supernatant and redispersion of the obtained pellet in phosphate buffer pH7 2mM until a final volume equal to the initial volume was attained.

Control samples were also made: 1) a blank control (no addition of EDC/NHS and Gra6 II, and no centrifugations were made) entitled from now on as CS, and 2) an EDC/NHS control (no Gra6 II addition steps were made) entitled from now on as CF.

For characterization via UV-Vis, DLS, and ELS dilutions of 150 μL of nanoparticle solution dispersed in 850 μL of phosphate buffer pH7 2mM were used; for NTA dilutions of 50 μL nanoparticle solution in 950 μL of phosphate buffer pH7 2mM were used.

Results and Discussion

1.50 nm Nanospheres synthesis and functionalization

1.1 Non-toxic and surfactant-free synthesis of approximately 50 nm nanospheres – A step-by-step creation.

The first ever synthesis of colloidal gold utilizing citrate as a reduction agent was first introduced by Turkenvich et al. in 1951 [130] and later improved by Frens et al. approximately 2 decades later[131, 132]. In this reaction, hot gold (III) ($HauCl_4$) solution and trisodium citrate are the reactants, having the trisodium citrate a double function as both a reducing agent, allowing the gold (III) to be transformed into gold (0) (Au^{3+} ions -> Au^0 ions), and as a stabilizing agent [133]. When the Au^{3+} ions are reduced into neutral Au^0 ions, the solution reaches a point of gold saturation, which leads to the deposition of noble metal particles[134], and the creation of gold nanoseeds, normally referred to as merely seeds. Citrate is reduced to 3-ketoglutaric acid and carbon dioxide. These side products can be removed using washing by centrifugation.

$$Na_3C_6H_5O_7\ (\text{trisodium citrate}) + 3H^+ \longrightarrow\ C_6H_8O_7\ (\text{citric acid}) + 3Na^+$$

$$2\ HAuCl_4\ (\text{hydrochloroauric acid}) + 3\ C_6H_8O_7\ (\text{citric acid}) \longrightarrow\ 2Au\ + \\ 3C_5H_6O_5\ (3-\text{ketoglutaric acid}) + 8HCl + 3\ CO_2$$

In this work, a seed-growth method was used for the nanospheres synthesis. The aforementioned seeds are used as crystallization nuclei in further steps of synthesis, allowing for a more controlled size and shape of the final product. After a seed creation step, growth-enabling solutions containing more $HauCl_4$ and trisodium citrate are added as needed. The newly introduced and reduced gold particles are then assembled at the

surface of already established Au seeds, due to changes induced into the solution via temperature decrease which does not allow new seeds to form. The growth steps can be repeated until the desired size is obtained. It is to note that this type of synthesis is extremely sensitive to external stimuli. Not only the reactant ratios should be as exact as possible, for even small changes to the ratios, such as the ratio between gold molecules and trisodium citrate may lead to different sizes and concentrations of gold nanoparticles [135], such as higher ratios of trisodium citrate:Gold nanoparticle leading to an increase in size and polydispersity[126]. Stimuli such as temperature are also to be controlled during the whole duration of the synthesis, for differences in its value may lead to differences in the final product. Example of that is the temperature for the obtainment of gold nanoseeds is around or above 100° C, however, for the growth steps the temperature used is around 90° C, as such temperature allows for the growth of the nanoparticles in size but does not allow for the creation of new seeds[36, 126]. Yet, such refinements allow for a specific tailoring for the sizes and concentration of gold nanoparticles one wants to obtain, giving a great advantage in the use of such method when obtainment of specific sizes is desired.

The final colloidal suspensions of nanospheres were characterized by UV-vis and DLS, to confirm that the desired properties were obtained. The results are shown in Figure 8, and Tables 1 and 2. In this work, nanospheres normally presented a range between 47 to 50 nm of diameter post-synthesis and concentrations that ranged from 10 to 15 nM ($nmol*dm^{-3}$), which were approximately the sizes we were looking for, when measured via UV-Vis spectrophotometry. Via UV-Vis it is possible to obtain the size of metal nuclei of the nanoparticles, without a significant contribution from the capping corona[129].

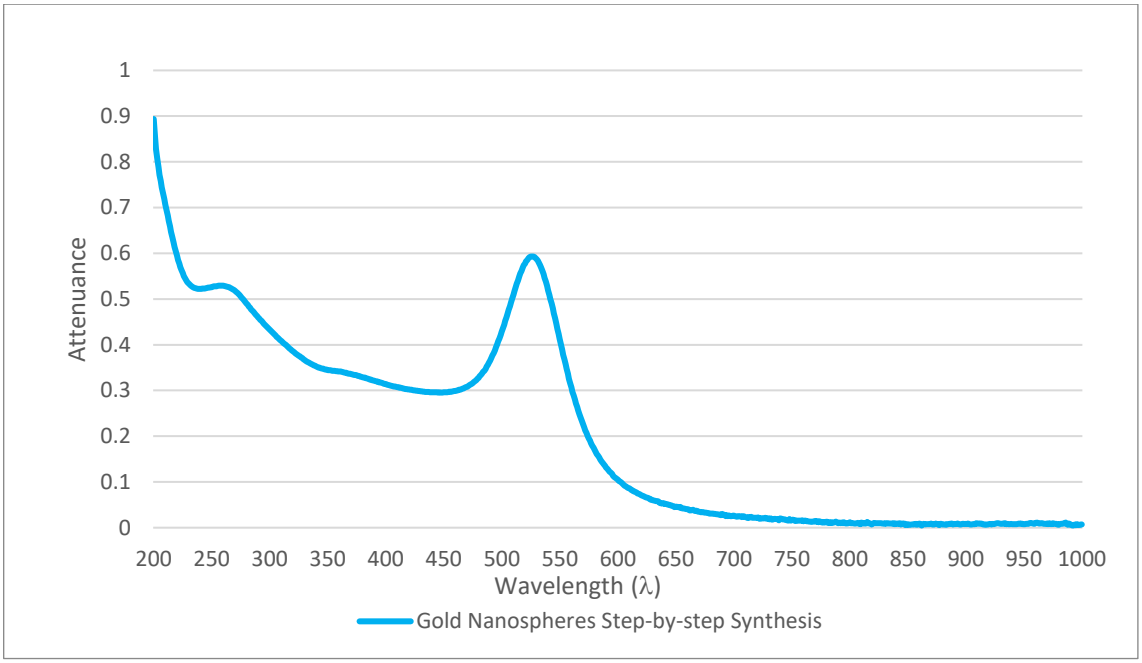

Figure 8 – Representative UV-Vis spectrum of gold nanoparticles of ≈ 50 nm, in aqueous suspension.

With the presented figure some key characteristics are possible to be observed: I) the spectrum presents a peak at approximately 525 nm, which is a the characteristic wavelength for 50 nm diameter nanospheres; II) the band presented in the figure is narrow, which indicates a low dispersion of sizes; III) no more peaks or elevations of the graphical curve are detected at higher wavelengths, which indicates that no significative aggregation of nanoparticles was observed. As such, its possible to infer that a monodisperse solution of nanoparticles of 50 nm of diameter was successfully obtained [128].

Table 1: Diameter and concentration of the AuNPs obtained from UV-Vis spectra.

UV-Vis Data	
Sample name	Gold Nanospheres Step-by-step Synthesis
Maximum attenuance	0.5931
Wavelength at maximum attenuance	527 nm
Attenuance value at λ = 450 nm	0.2958
Diameter (nm)	46
Concentration (nM)	0.15

Concurrently to the analysis via UV-Vis spectrophotometer, DLS and ELS measurements were also performed. to determine hydrodynamic diameter, polydispersity index (PDI) and, and zeta potential. The results are shown in Table 2.

Table 2: Dynamic light scattering (DLS) and electrophoretic light scattering (ELS) characterization of AuNPs.

DLS and ELS Data					
Sample name	Gold Nanospheres Step-by-step Synthesis				
Particle Average size (nm)	40.93	41.64	42.02	42.48	42.62
Polydispersion Index	0.133	0.150	0.160	0.152	0.154
Particle Zeta Potential (mV)	-33.7	-35.4	-36.7	-37.7	-38.6

Table 3: Table representing the two synthesis of nanospheres of size approximately 50 nm. In the table the deviation values are presented as a way to show the repeatability of the synthesis obtained.

	UV-VIS				
Sample	λMax	nm (λMax)	λ450	Size (nm)	Concentration (nM)
AuNP VT	0.620	525	0.303	52	0.11
AuNP VT II	0.593	527	0.296	46	0.15
Deviation Values	0.0133	1	0.00352	2.833	0.0197

First of all, in DLS analysis the average particle size is normally bigger to the particle size obtained via UV-Vis, because while UV-Vis indirectly measures the diameter of the gold metallic core of the nanoparticles, DLS measures the average hydrodynamic diameter of the nanoparticles, i.e. it includes the capping agent and the hydration layer[136, 137]. DLS also measures the size dispersion of the samples as polydispersion index, PDI. Monodisperse samples have PDI values lower than 0.2[128]. Higher values indicate nanoparticle aggregation. Nanoparticle aggregation is very important to avoid, since it can lead to incomplete functionalization of the nanoparticles, and thus lower efficiency in their utilization for a SERS type test employing biological samples. Finally, zeta potential is a measure of the electrical charge at the surface of the particles; such charges become of great importance when functionalizing and employing the nanoparticles, being needed to have in mind the charges of the reactants in functionalization or of the molecules in the medium so that the desired reactions may work in the most favourable way possible[138, 139].

As seen in table 2, the data obtained in our analysis both in UV-Vis, DLS and ELS present the expected results, with PDI values below 0.200. Therefore, it becomes possible to say that such nanoparticles present great prospects for next functionalization steps. However, before further functional functionalization for the creation of our desired nanoprobes may continue, an additional step is needed: the

substitution of trisodium citrate as a protector group, for a new protector group that not only binds in a stronger way to the nanoparticles, but that also allows for a higher protection to them, be it's in reactions but also in physiological media[140-142].

1.2 PEG as a capping and functionalization group for nanospheres – an amphiphilic capping agent

As mentioned before, trisodium citrate in solution did not only reduce the Au^{3+} ions into neutral Au^{0} particles, but also serves as a protecting agent to the newly synthesized nanospheres. However, for the preparation of the nanoprobes, the citrate protective group on the synthesized nanospheres must be substituted by a PEG group (Figure 9), leading to a step of PEG functionalization, also known as PEGylation. This step is required because: i) the utilized PEG presents a thiol group (-SH), which allows the molecule to bind much more strongly to the gold nanoparticles due the high binding affinity verified between gold and -SH, allowing then a higher protective power for any chemical impurities in the solution[108, 143-146]; ii) the utilized PEG in this work presents a terminal carboxylic group (-COOH), which is of high importance for the successful binding between the nanoparticles and Gra6II due to it presenting a terminal amine group ($-NH_2$)[16, 79, 147]. Such importance and mechanics of such step will be further detailed ahead in the chapter “Functionalization of PEGylated nanospheres via EDC/NHS activation – creation of a gold nanoprobe for detection of Toxoplasmosis”; (iii) PEG molecules present a high biocompatibility in biological and physiological medium due to its capacity to reduce non-specific binding of proteins and other biomolecules, while acting as a stealthing agent[68, 71-73, 148], in other words, it allows for the nanoparticles to remain in physiological and biological mediums for higher periods of time, without any significant interactions with proteins in the media, making them as perfect candidates for use when utilizing biological and physiological material.

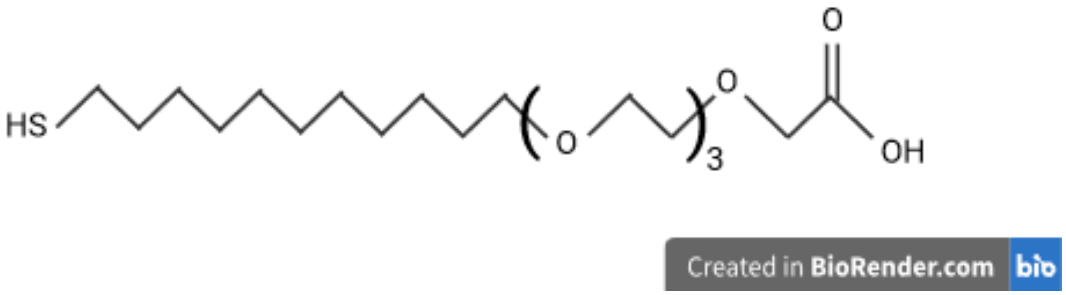

Figure 9 – Structural formula of the SH-PEG-COOH molecule used.

Due to PEG having a stronger binding strength to the nanoparticle than citrate, the PEG molecules substitute the citrate molecules in the surface of the nanoparticles forming a covalent bond[65, 71, 73, 140, 141]. The citrate capped nanoparticles were incubated in the presence of PEG, and centrifugations post incubation and pellet resuspension in buffer allows for the removal of citrate from the system. Several ratios of PEG:AuNP were analysed to better utilize the PEG molecule and its protective capacity. From the results obtained via UV-Vis spectrophotometry it becomes possible to conclude: 1) Amongst the samples that were centrifuged the CF presents a significative descent in attenuance value. This may be indicative of some stronger protection properties that PEG exerts in the AuNP when compared with using citrate as a protection group; 2) the introduction of different ratios of PEG:AuNP leads to different attenuance values of different samples, as can be clearly verified in the graph with the sample ratio of 57800. This means that different concentration ratios of PEG:AuNP can lead different results (Figure 10 and figure 11), therefore a careful selection of which ratios to advance the work with is also needed.

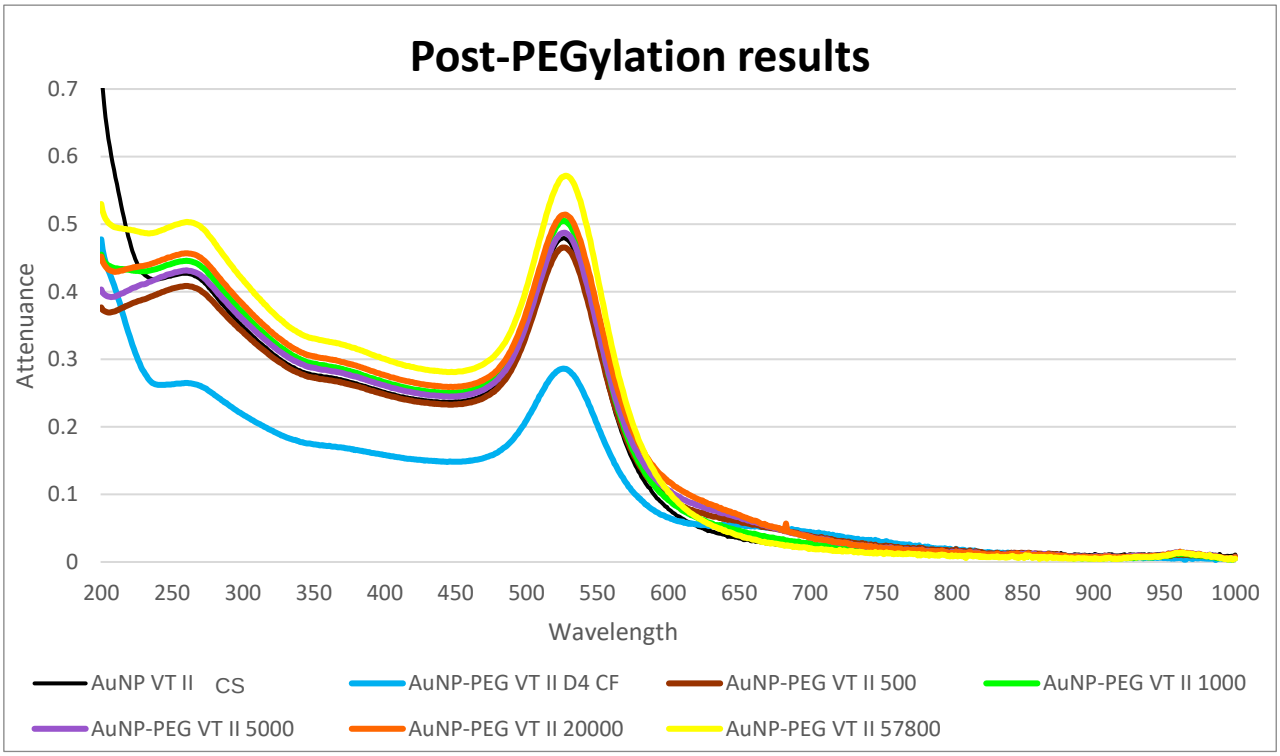

Figure 10 – Graphic obtained via UV-Vis spectrophotometer of all samples of concentration ratios of PEG:AuNP (500, 1000, 5000, 20000, 57800) and controls (CF and CS (Blank)). All samples used the same dilution for the characterization, meaning that in the CF sample there was a loss of nanoparticle material.

When analysing the DLS and ELS characterization parameters values (figure 11), it becomes possible to further extend not only our understanding of how the PEG molecules reacted with our AuNP, but also give us further information to allow for a good choice of ratios to use for further work.

No significant changes in AuNP-PEG hydrodynamic size were seen, which is in accordance with other works which indicate that PEG molecules in gold nanoparticles do not affect its hydrodynamic size [95]. Yet, most notable is the substantial changes in PDI amongst samples. First the PDI increasing slightly and then decreases, leading to smaller values of PDI to be observed in the concentration ratio of 57800, which present values that prove themselves of good value to further use in future protocols due to being not only the smallest PDI value obtained but also being a value under 0.2, which presents itself in literature as a good value while maintaining the highest value of attenuance. Zeta potential values also presented small differences, this may be due to action of the PEG, leading to an increase of the zeta potential of the AuNP-PEG; however, increasing the PEG concentration ratios causes a decrease in the Zeta potential. Such may be due to the fact that the more concentrated PEG becomes in the surface of the nanoparticles, the less of the interior of the molecules becomes

positioned in a manner that may change the surface charge of the AuNP-PEG complex.

Upon analysing the data, the concentration ratio of 57800 was selected as the one to be used. This due to I) it's low PDI value overall obtained via DLS and ELS analysis concomitantly with the identifiable lack of aggregation of nanoparticles via UV-Vis spectrophotometry, and II) the peak attenuance value obtained UV-Vis, which indicates a superior capacity to serve as optical test base for a SERS type test due to the higher attenuance value obtained in comparison with the other used samples, suggesting a superior optical signal response to alteration to the nanoparticles, such as target molecules binding relatively to the remaining samples.

a

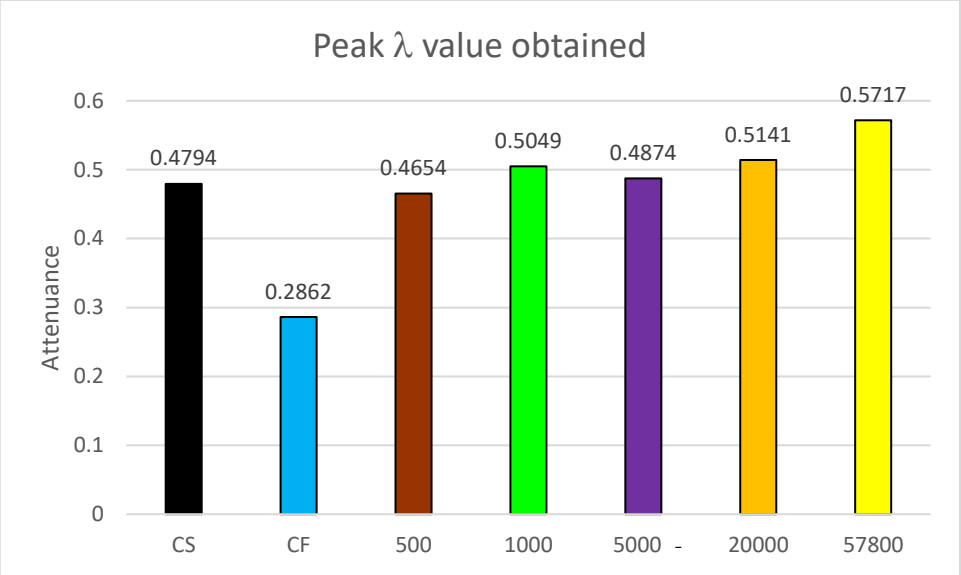

b

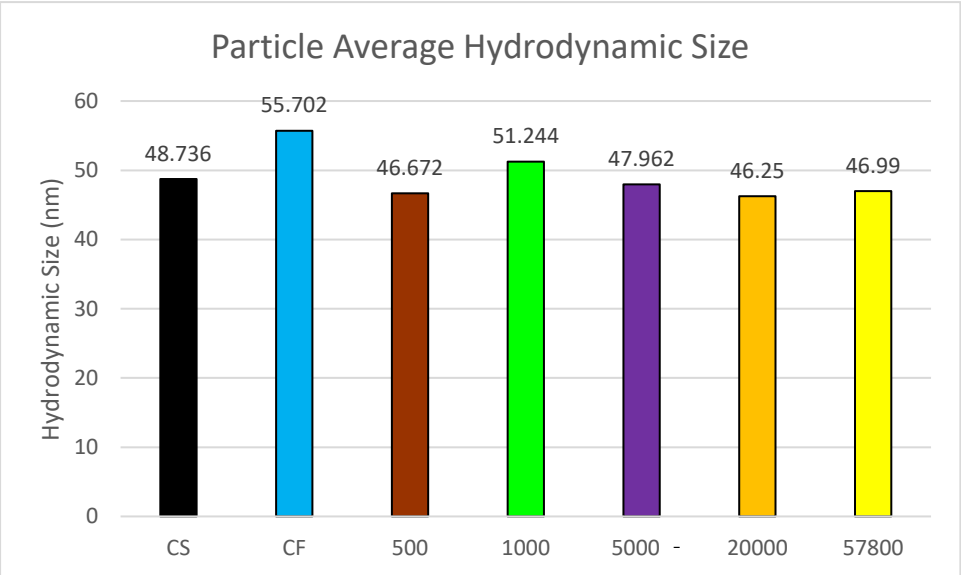

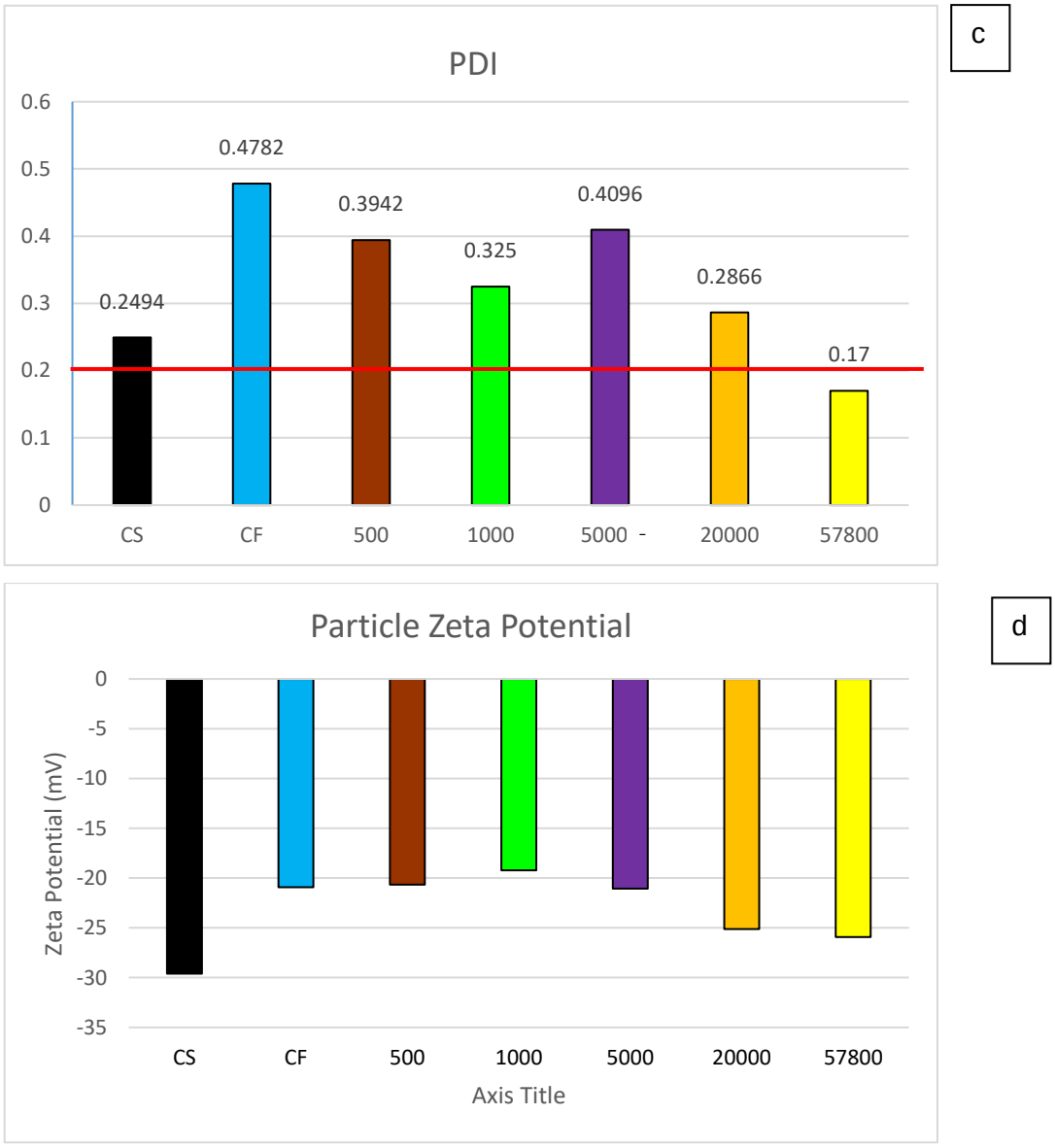

Figure 11 – Visual representation compilation of the most important characterization parameters data obtained via DLS (particle average hydrodynamic size (11b) and PDI (11c)), ELS (particles zeta potential (11d)) and UV-Vis (peak λ value obtained (11a), utilizing the tables average values for each parameter analysed post-PEGylation process. Such was done to simplify the process of data analysis in cases of large disparities of values amongst the same parameters. In the PDI graph a bar identifying the 0.2 value was added to facilitate the identification of remarkable PDI values.

1.3 Functionalization of PEGylated nanospheres via EDC/NHS activation for Gra6II binding – creation of a gold nanoprobe for detection of Toxoplasmosis.

After the PEGylation step, now comes the question of how to bind the Gra6II synthetic peptide. Many solutions are available to do such, however, one technique in specific has been used in several fields of nanotechnology especially those pertaining to the creation of nanoparticle-based disease detection tests and similar nanoparticle-based tests, being those that technique of carbodiimide chemistry, also known as EDC/NHS chemistry binding.

EDC/NHS chemistry serves as a mediator linker between the AuNP-PEG which presents a -COOH group and Gra6II which presents an -NH_2 group[44, 62, 75, 76, 149-151]. The EDC is added first and reacts with the carboxyl moiety to form an intermediate compound, O-acylisourea[76]. The intermediary compound is highly reactive, and reacts extremely fast with an electron donor, i.e., a nucleophile, being such nucleophile either a primary amine, such as the one present in the Gra6II peptide, or an oxygen atom from the water used as a dispersant medium[76]. It's due to that reactivity that NHS is used in a second step reaction, allowing for a much more stable intermediary compound, improving peptide coupling efficiency[75, 149, 151]. The NHS reacts with the EDC and forms an ester, more specifically an amine reactive NHS ester, that stays attached much strongly to the AuNP-PEG due to this intermediary being hydrophilic and hydrolysing in a much more slowly way relatively to O-acylisourea, allowing for a much more stable intermediate compound[76, 149]. When the Gra6II peptide is later introduced into reaction medium, its primary amine nucleophile rapidly hydrolyses the intermediary ester, and allows the formation of a covalent amine bond[76], as can be seen in figure 12.

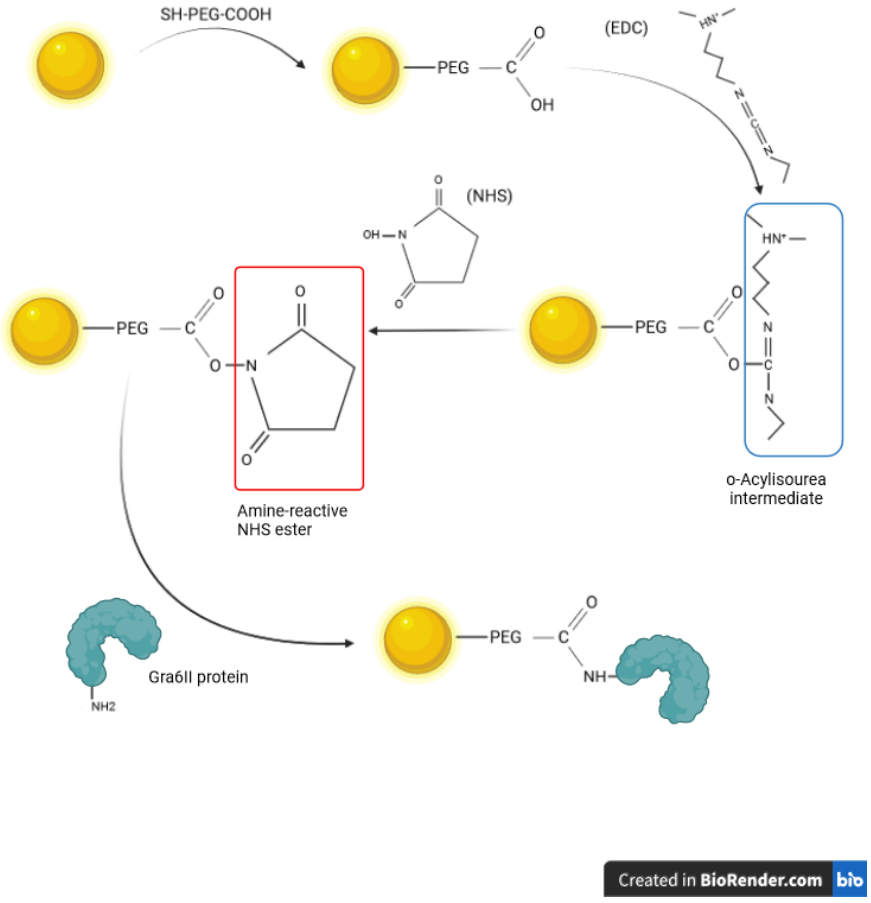

Figure 12 – Scheme of the steps of AuNP functionalization. Each reactant addition and intermediary compound is represented on the image.

After preliminary testing, the selected final volumes of EDC and NHS to be used for the functionalization of the AuNP-PEG used in this work was obtained.

Due to the nature of the mechanisms of actuation of EDC/NHS technique, it may lead to aggregation of nanoparticles when used in excessive concentrations. As such the samples are to be measured via UV-Vis to verify the best concentrations to used (figure 13). In this work a final concentration of EDC of 3 μM and a final concentration of NHS of 6 μM were used, presenting the best values amongst the tested concentrations. Via figure 13 it becomes possible to observe that amongst the two final concentrations studied, the selected one presents two crucial selection factors: I) the selected concentration of 3 μM of EDC and 6 μM of NHS presents the best peak attunement value, for presenting the higher attenuance value and low aggregation potential; and II) the selected concentration does not present significant aggregation as can be verified in the graph obtained, however it becomes possible to verify that clusters of aggregation are becoming more liable to appear in higher concentrations of

the pair of reactants, therefore higher concentrations are not advised to be further studied, and to avoid aggregation.

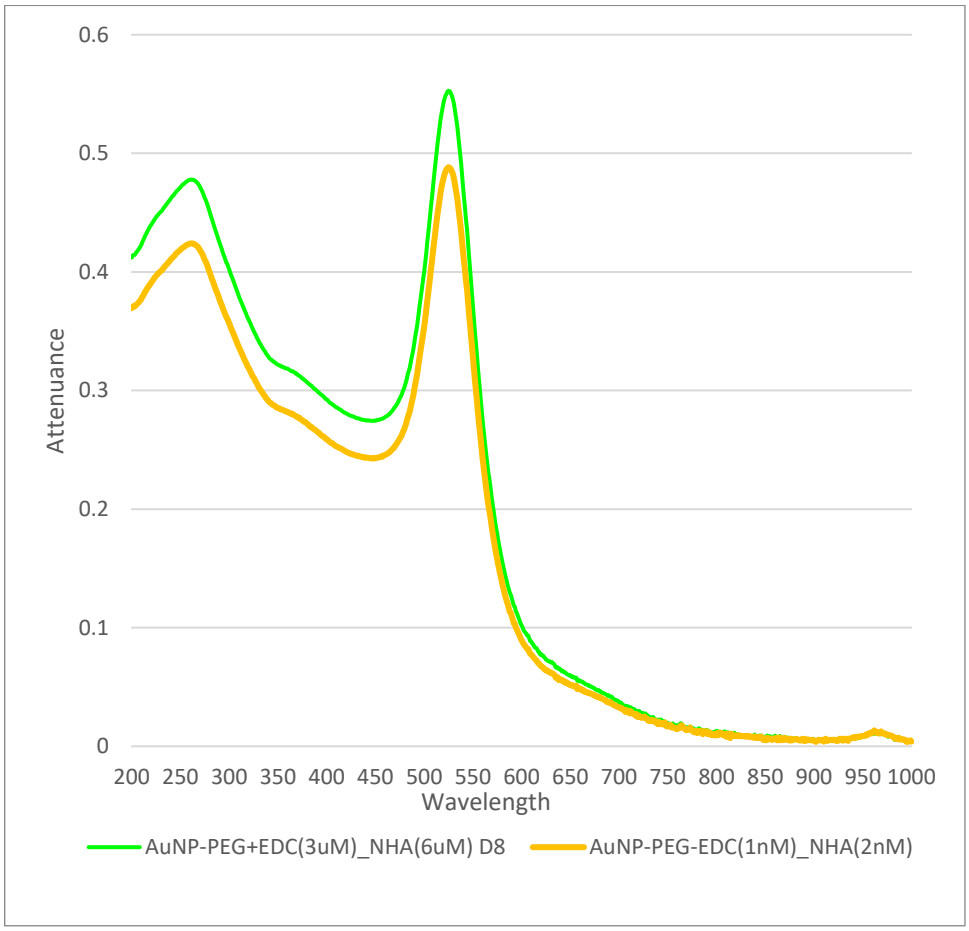

Figure 13 –UV-Vis spectra of the preliminary tests of concentrations off EDC and NHS to be used. 2 final concentrations of the pair of reactants (EDC and NHS) were made, always with a ratio of EDC:NHS of 1:2. The final concentrations utilized were: 1) 3 μM of EDC and 6 μM of NHS, and: 2) 1 nM of EDC and 2 nM of NHS.

Once the most appropriate concentrations was selected, the covalent binding of Gra6II to the AuNP-PEG was performed. Anew, tests were made at different concentrations of Gra6II:AuNP, being such concentrations: 1000; 5000; 7500; 10000; 25000; 50000. Two controls were used, such as in previous tests, the CS and CF controls (figure 14, figure 15, and figure 16).

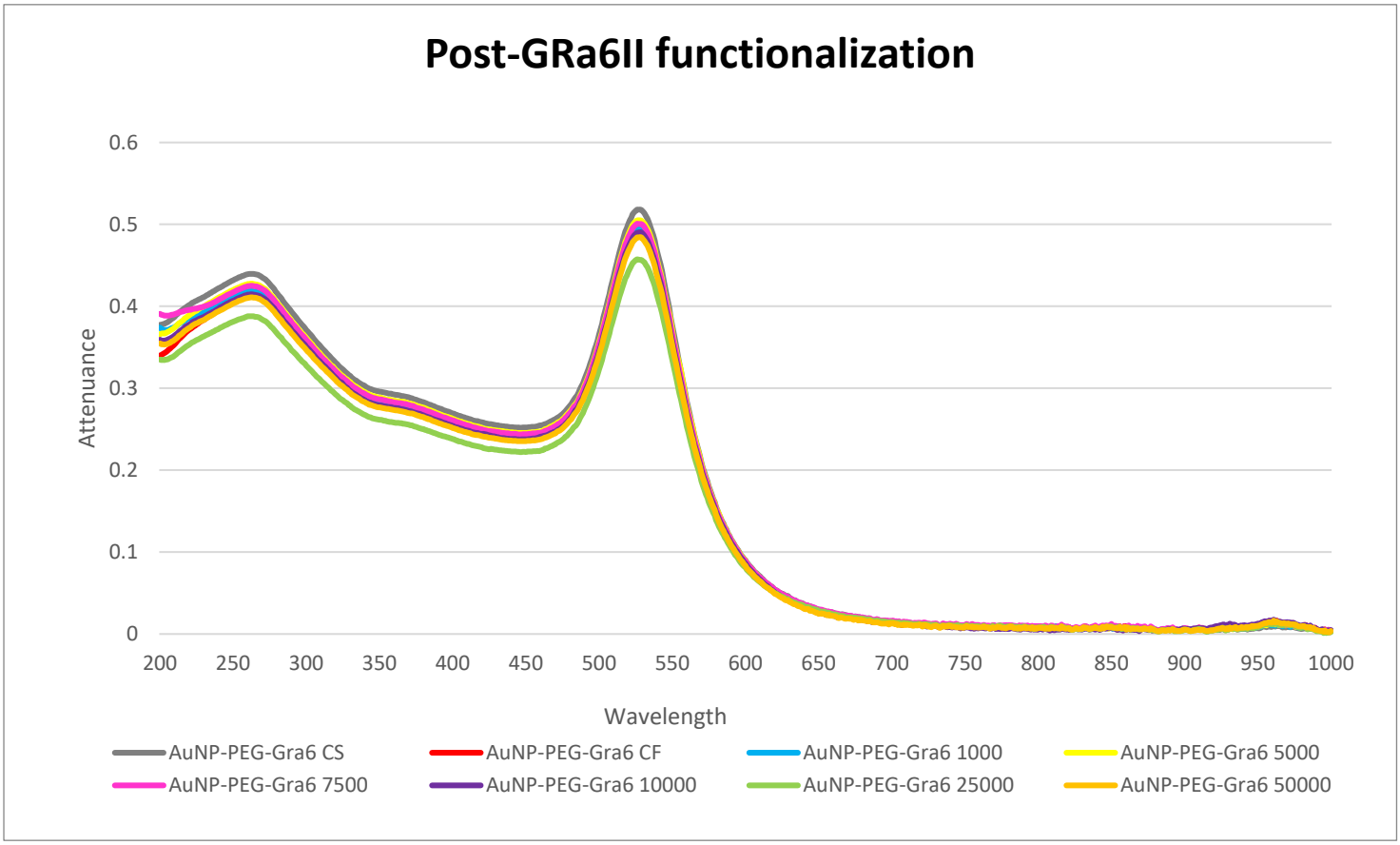

Figure 14 – Graphic obtained via UV-Vis of AuNP-PEG post EDC chemistry and successive Gra6II binding.

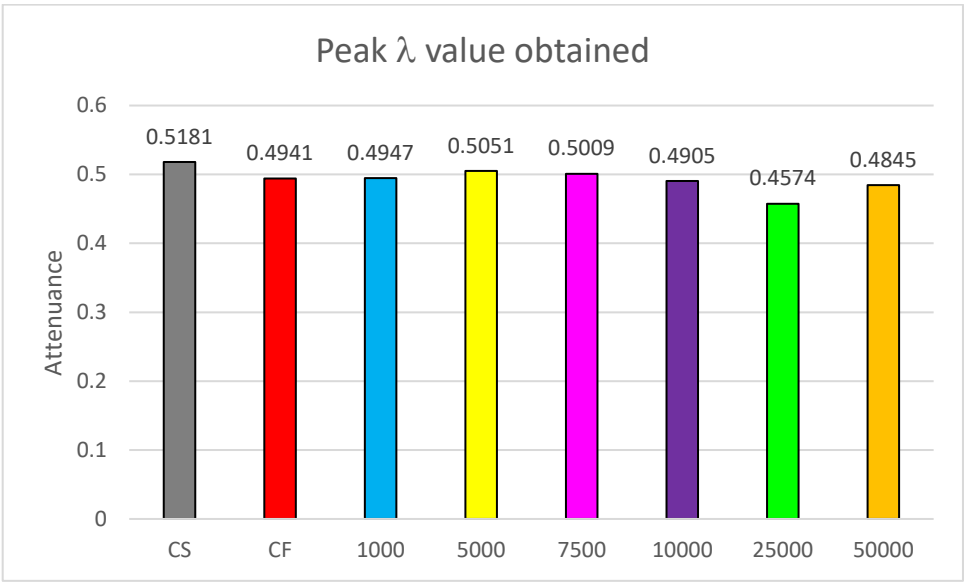

a

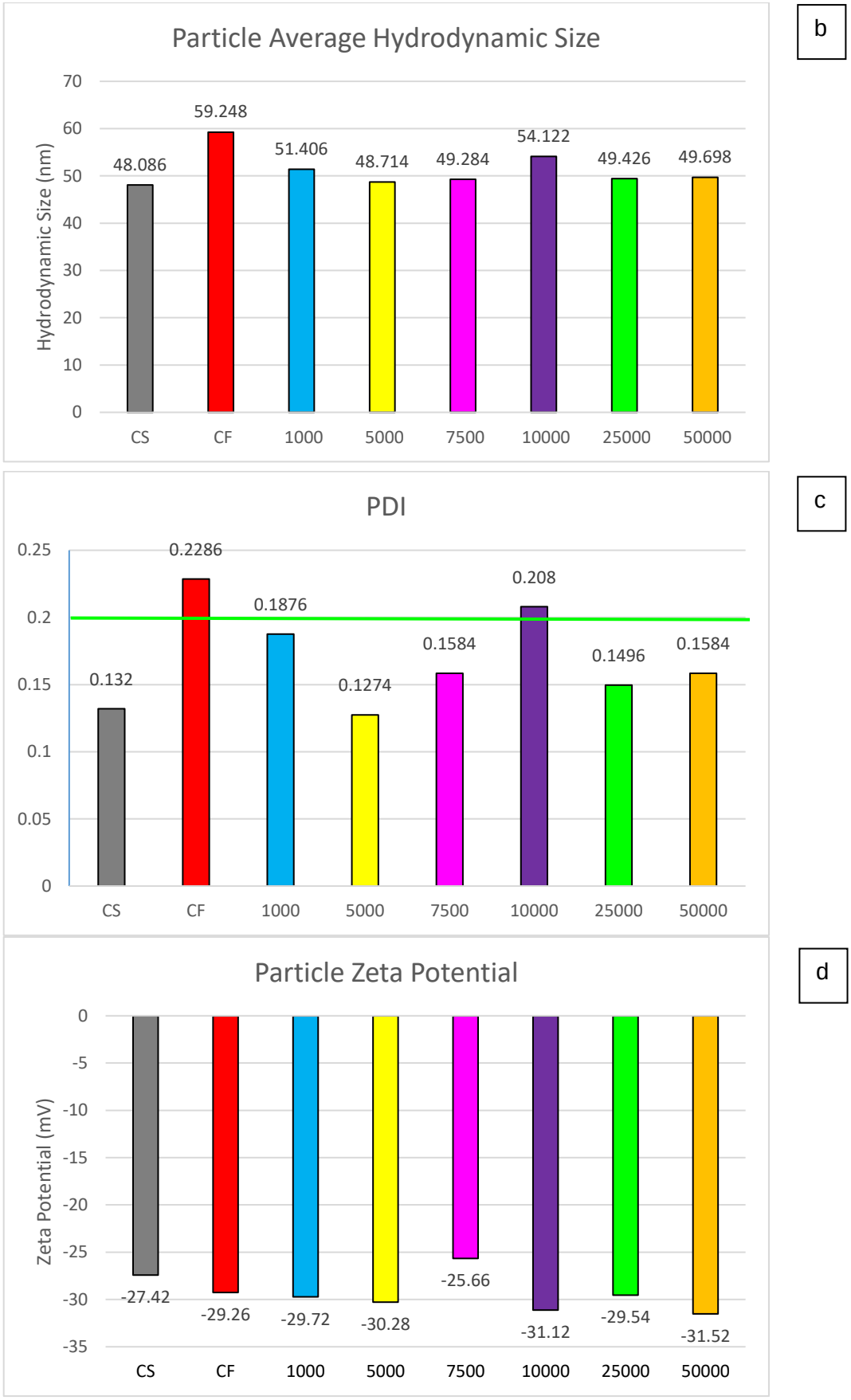

Figure 15 – Visual representation compilation of the most important characterization parameters data obtain via DLS (particle average hydrodynamic size (15b) and PDI (15c)), ELS (particle zeta potential (15d)) and UV-Vis (peak λ

value obtained (15d)), utilizing the tables average values for each parameter analysed post EDC chemistry and Gra6II binding to the AuNP-PEG. The CS control corresponds to the values obtained previously in sample 57800 ratio presented in the chapter “Usage of PEG as a protector and functionalization group for nanospheres – an amphiphilic protector”, this due to the fact that such ratio was the one selected to proceed to the peptide binding phase.

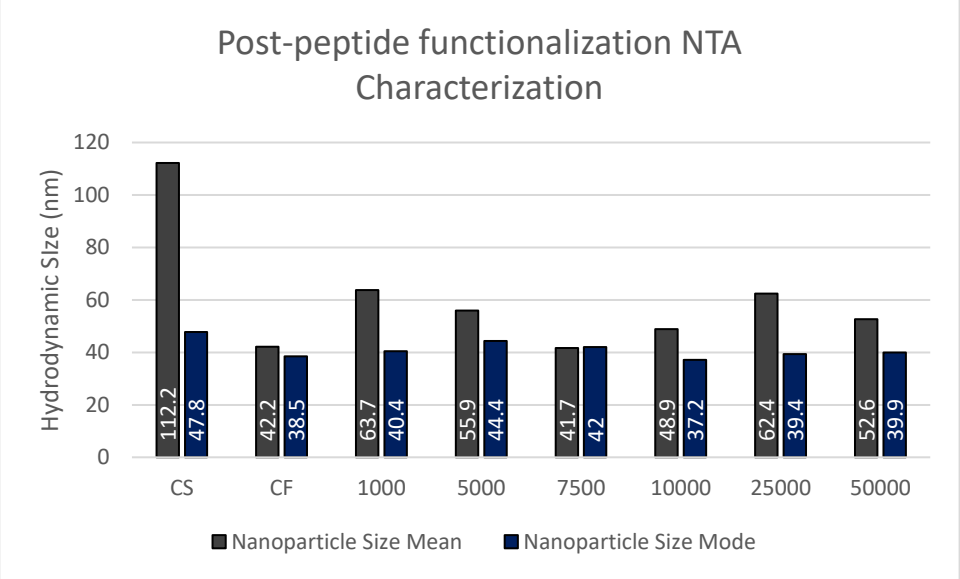

Figure 16 – Data obtained post NTA characterization. The utilized characterization parameters analysed where nanoparticle hydrodynamic size mean and nanoparticle hydrodynamic size mode.

By analysing the values in figure 15, it became possible to select the most appropriate ratios of Gra6II to use. A small decrease in the peak λ value obtained in the PEGylated nanoparticles presenting Gra6II functionalization (AuNP-PEG-Gra6II) when compared to the CS control (which is the AuNP-PEG ratio 57800 presented in the last chapter), such being a possible indication that binding of Gra6II was successful.

The DLS and ELS data also seems to verify such; I) the average size of nanoparticles obtained seem slightly bigger than the ones obtained in the PEGylation experiments, however such change is not significant enough to delineate conclusions with a high certainty; II) a small increase in PDI was verified, which is expected of a successful addition of peptide. This is due that the addition of peptide leads to a decrease in monodispersity, for the peptide binding is not equal in manner in all gold nanoparticles, not only position wise, but also concentration of peptide:nanoparticle is not the same for each nanoparticle, thus leading to the verified decrease in monodispersity, which in turn is represented via a higher value in PDI; III) modifications in the zeta potential of the nanoparticles, in specific a decrease in surface charge, this

could be due to the amino-acid charges of the synthetic peptide that are located in an exterior and are modifying the overall surface charge, which would only be possible with a correct binding of peptide sequences to the nanoparticle.

A concomitant analysis via NTA was made to cross-analyse with the results obtained. Overall the results are of good consistency, amongst themselves and the DLS and ELS obtained results, even having into account some outliers amongst mean and mode results, that may be result from the high disparity amongst the mean and mode verified in the CS control, which may be a consequence of the time passed between the synthesis and utilization of the nanoparticles, for the stability and shelf-life of the nanoparticles is dependent of such parameters as time, temperature, pH and many others.

Therefore, it seems that the results overall are good, however considering time and budget constraints a small number of ratio concentrations needs to be selected for further experimentation. As such, the concentration ratios selected were the ones corresponding to the ratio 5000 and the ratio 50000, to better understand if onwards experiments may present differences between a small concentration ratio and a high concentration ratio of Gra6II:AuNP (figure 17).

With the ratios selected new samples only utilizing such ratio were made, to verify the selection of the ratios and creation of batches for further studies.

a

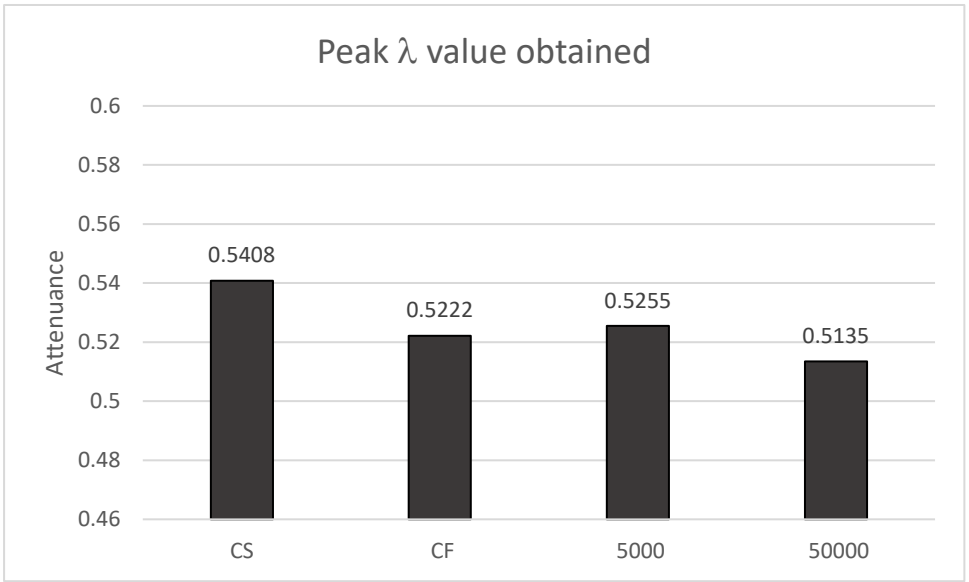

b

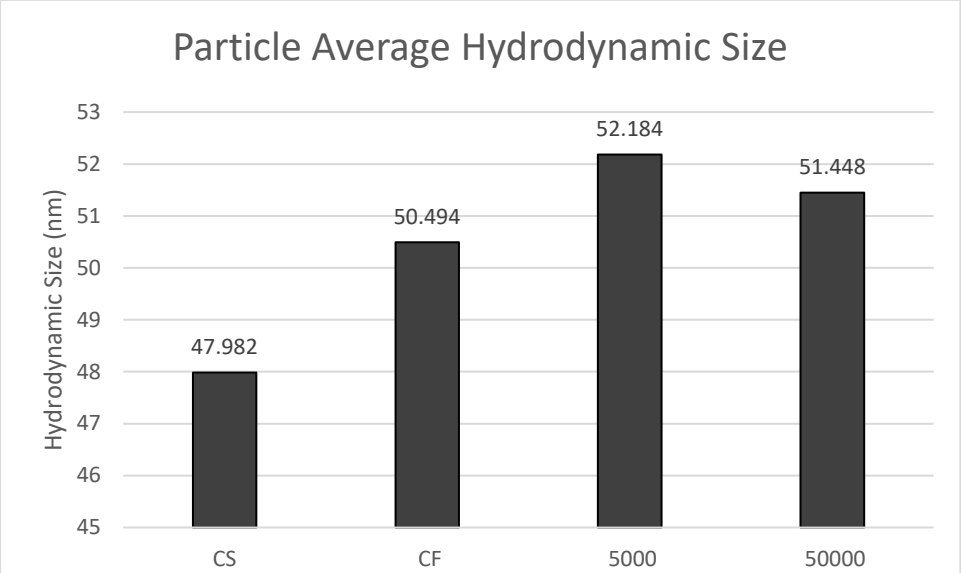
Particle Average Hydrodynamic Size
Hydrodynamic Size (nm)
53
52
51
50
49
48
47
46
45
47.982
50.494
52.184
51.448
CS
CF
5000
50000

c

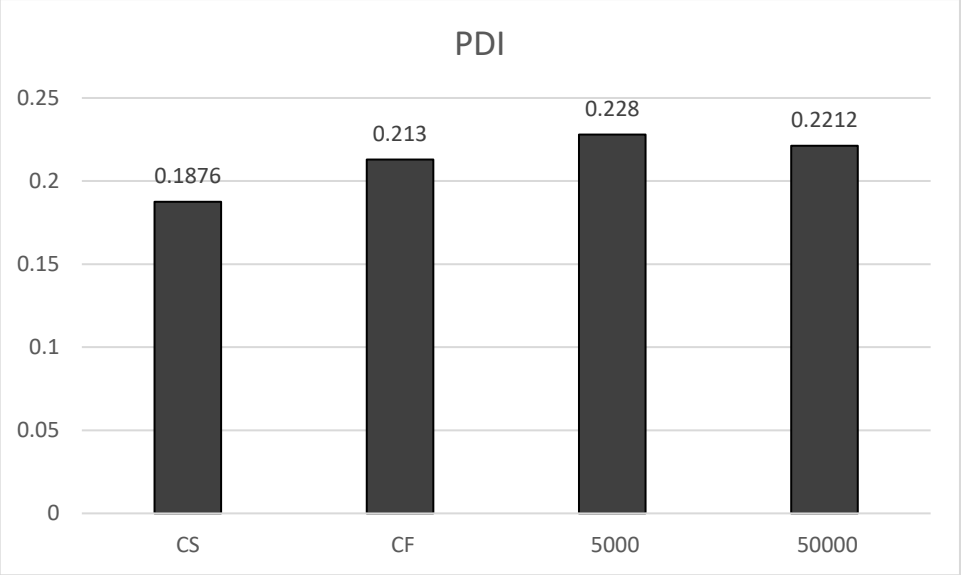
PDI
0.25
0.2
0.15
0.1
0.05
0
0.1876
0.213
0.228
0.2212
CS
CF
5000
50000

d

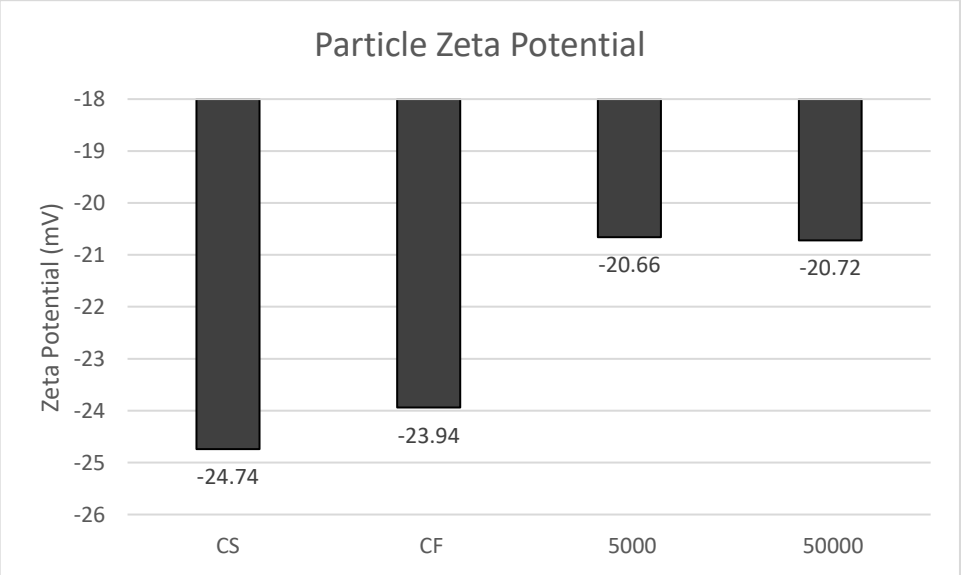
Particle Zeta Potential
Zeta Potential (mV)
-18
-19
-20
-21
-22
-23
-24
-25
-26
-24.74
-23.94
-20.66
-20.72
CS
CF
5000
50000

Figure 17 – Visual representation compilation of the results obtained of the newly selected concentration ratios via UV-Vis (17a), DLS (17b and 17c) and ELS (17d). Once again, the CS control corresponds to the AuNP-PEG ratio 57800 used in the peptide binding process via EDC/NHS chemistry.

Results of the same type between the CS control and then samples as before were obtained: I) a slight decrease in the peak λ value could be observed; II) a slight increase in the particle average size is not only also again identified, but is also more prominent; and finally, III) the PDI suffered, as expected, a small increase in value.

The results now obtained present themselves as a good basis for onwards works.

1. Nanostars synthesis and functionalization

2.1 Nanospheres versus nanostars – from lightning rods to shining stars.

Gold nanostars (AuNS) also present highly controllable morphology during synthesis via control of $AgNO_3$, which functions as a regulator of the direction of growth of the branches of the nanostars and L-Ascrobic Acid, which functions as a growth agent[126]. Such reflects into a highly tunable plasmon resonance (SPR), for the control of the growth of the branches change the way the nanostars interact with the surrounding environment[88, 89]. In consequence, highly tunable localized surface plasmon resonance (LSPR), is an effect that define noble metal-based nanostructures[92, 95, 109, 152, 153]. LSPR differs from SPR due to LSPR being an extremely localized oscillation in solely the nanostructure and their hotspots, while SPR being an oscillation amongst the metallic-dielectric interface[109, 154]. As such, LSPR, when compared to SPR, presents a shorter field decay[155, 156], signifying a reduction to sensitivity of interferences from the medium refractive index fluctuations while also providing therefore, a much more increased sensitivity to changes on the noble metal (in this work, gold) nanostructures. Due to such, noble metals such as gold and silver present a high potential for the creation of nanoassays based on optical properties of the metallic nanomaterials in a panoply of areas.

Such tunability to LSPR is also capable to reach near infra-red (NIR) wavelengths[95], which is optimal for biological applications, supplementing to the

already described positive points that demark nanoprobes based immunoassays, as the one presented in this work, as optimal candidates for the elaboration of disease and pathogenic infections in humans and animals, in a much more expeditious and cost-efficient manner than many of the techniques available at this present time.

As such the optical responses of AuNS are extremely complex, for the existent anisotropic morphology caused by the branches in the nanoparticles[157, 158]. These branches lead to a presence of 2 simultaneous focalizations of EM existing simultaneously (figure 18): higher intensity EM localized in the tips of the AuNS and, lower intensity EM localized in the metallic core[155, 159, 160], being such theorized to be identifiable by the presence of 2 distinct LSPR bands, which are represented in spectrophotometry techniques as the existence of 2 peaks of different values. These 2 bands normally present values of wavelength approximately between 650-900 nm for the higher intensity band, and 500-600 nm for the lower intensity band[155, 160, 161]. Such enhancement and focalization of electric field on the tips of the branches leads to what is denominated as the “lightning rod effect”[162] and is theorized to be responsible for the optical signal amelioration of SER activity[155].

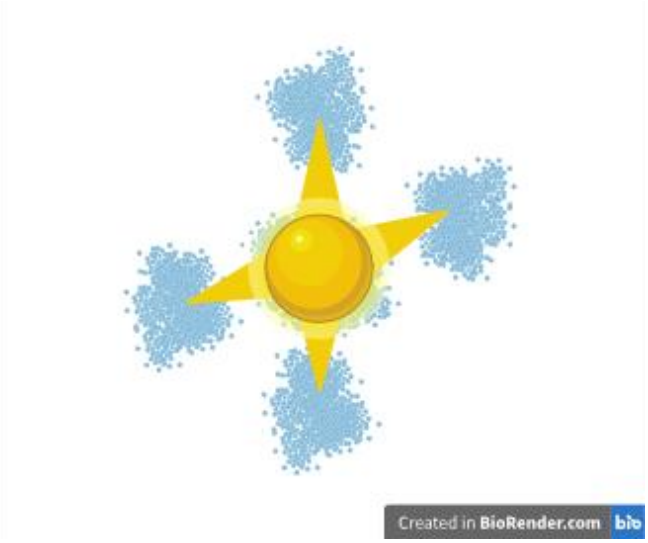

Figure 18 – Visual representation of the 2 points of EM focalization (presented in blue). The anisotropic nanostars (presented in yellow) present a high intensity EM focalization in the tips of the branches and a low intensity EM focalization in the metallic core of the nanoparticle.

For such reasons it is possible to assume that theoretically AuNS may prove to be a better alternative for the creation of the nanoprobes to be used in a SERS type immunoassay test for the identification of Toxoplasmosis anti-Gra6II antibodies in serum, due to their ameliorated optical signal strength when compared to AuNP.

2.2 Gold nanostars synthesis using a seed-mediated method – pressure makes diamonds and chemistry makes stars.

AuNS synthesis utilizes AuNPs of approximately 15 nm as a basis [67, 135]. To that basis additions of $HAuCL_4$, to be reduced to allow for the addition of gold particles to the already synthesised seeds, and a duo of L-ascorbic acid and Silver Nitrate ($AgNO_3$) that are used at the same time, being that the L-ascorbic acid acts as the reducing agent of the gold (III) into gold (0) (as explained in chapter “Non-toxic and surfactant-free synthesis of approximately 50 nm nanospheres – A step-by-step creation.”) and $AgNO_3$ acts as an interloper via the creation of the anisotropic branch growth in the nanoparticles, which characterize AuNS morphology.

A precautionary note should be added that L-ascorbic acid and $AgNO_3$ should always be added at the same time, for if the Ag^+ ions, originating from the $AgNO_3$, are introduced too soon to the medium, silver chloride salt will precipitate and no nanostars be added upon addition of L-ascorbic acid[135]. In the same manner, if Ag^+ ions are introduced too late in the medium, most of the gold will have become reduced and has already deposited itself and formed larger spheres from the addition of L-ascorbic acid, becoming then the function of Ag^+ ions compromised, and no branches being successfully synthesized[135]. Environmental external stimuli such as pH, temperature and others should be highly controlled. During this work some changes in protocol for the nanostars had to be made, such as temperature. Initially the synthesis for gold nanostars was made at room temperature, however that proved ineffective to obtain reproducibility of synthesis, being such normal according to literature[110]. Seeing as reproducibility of nanostars synthesis increases as the ambient temperature decreases[135], therefore after the original protocol was altered so the synthesis was made in a cold bath consisting of water and ice, which would set the temperate at approximately 1 to 3 ° C.

Therefore, such used technique allows for the formation of a surfactant-free AuNS synthesis that presents high plasmon tunability.

In figure 19 the graph obtained via UV-Vis, with the characteristics intrinsic to nanostars may be observed.

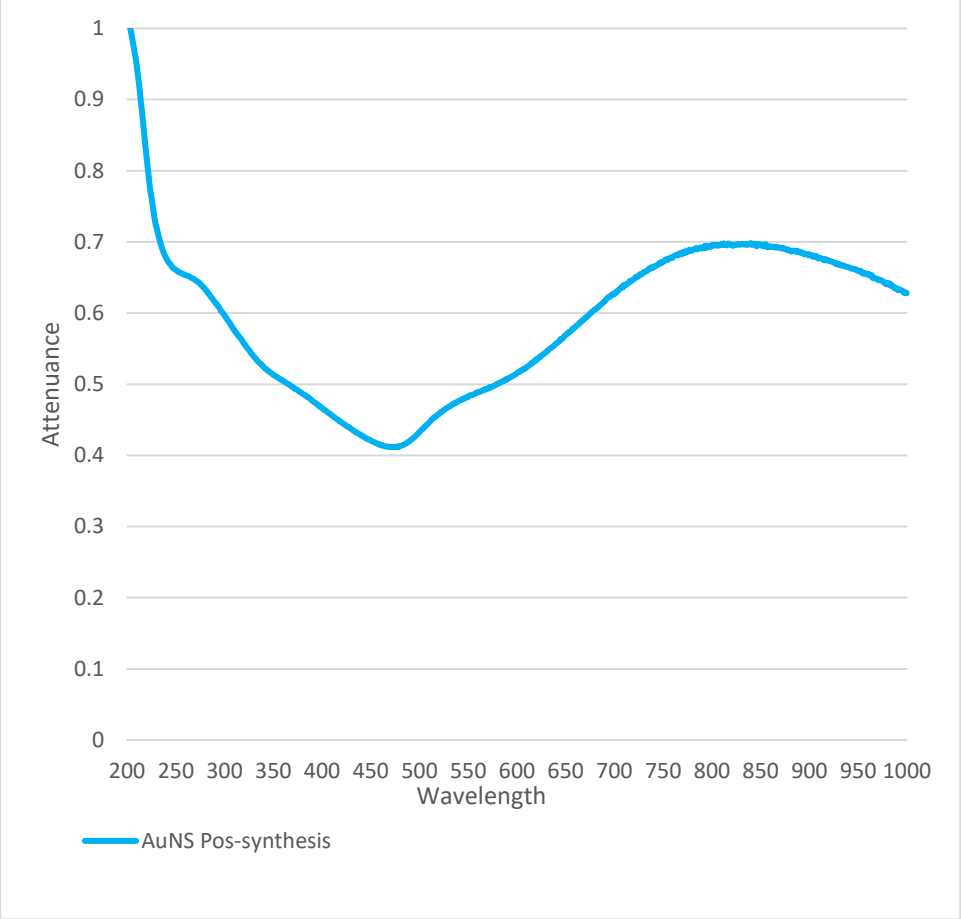

Figure 19 - UV-Vis graph obtained post-UV-Vis spectrophotometry of gold nanostars immediately post-synthesis. In the graph it becomes possible to verify the characteristics of a successful nanostar synthesis: 2 LSPR peaks are observed, the first at a wavelength approximately of 500 nanometres and another at a wavelength of 800 nanometres, which represent respectively the LSPR wavelengths characteristic of the nanostar nuclei and the nanostar branches tips.

2.3 PEG as a capping agent for nanostars – Nanospheres vs nanostars.

In AuNS the mechanism of functionalization works in the same manner that of the nanospheres, as the same type of PEG, specifically an SH-PEG-COOH, is utilized. The thiol group in the PEG molecule allows the PEG to bind to the surface of the gold nanostars[36, 78, 94, 144, 146]. However, a significant alteration that could be verified was the concentration ratios of PEG:AuNS. When using concentration ratios equal or superior to 50000, the particles would aggregate during incubation, being the

precipitation of nanostars aggregation visible at the bottom of the container. This signifies that nanostars present a higher sensibility to chemical aggregation when in reaction with other molecules, which has been reported before[98]. As such, different concentration ratios had to be utilized instead, being such concentration ratios of 500, 1000, 5000, 20000, 30000, 40000 and 50000 of PEG:AuNS. CS and CF controls were also utilized in all studies, being the characteristics of such controls the same as the ones in chapter “1.2 Usage of PEG as a protector and functionalization group for nanospheres – an amphiphilic protector.”.

Only concentration ratio 50000 presented slight visual aggregation. Upon analysis it became apparent that the saturation limit before any kind of aggregation of nanostars was a concentration ratio of 40000. As such, due to the saturated limit of the nanospheres being a concentration ratio of 57800, a concentration ratio of 40000 was selected for further studies done with nanostars. As such, comparison amongst the two morphologies is easier is both are in the same state of relative saturation.

The UV-Vis resulting graph may be seen in figure 20 and figure 21.

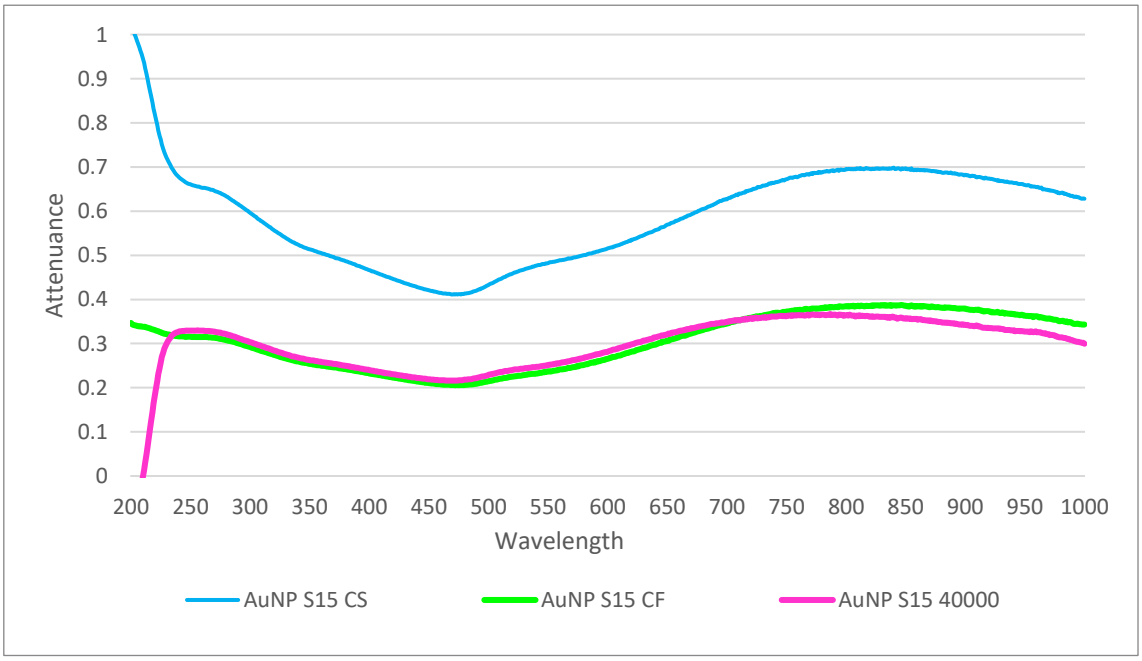

Figure 20 - UV-Vis graph obtained post-UV-Vis spectrophotometry of the different concentrations ratio of PEG:AuNS post-PEGylation. In the graph it becomes possible to verify that although the attenuance value suffered a slight decrease in value upon the PEGylation process, the shape of the obtained band and the location of the peak wavelength value only changes slightly (the peak wavelength value passed from 800 nm in the CS to 788 nm in the

concentration ratio of 40000). The reduction in the attenuance values of the samples CF and 40000 may be explained due to the high sensibility of the nanostars, there is a possibility that some material was lost, leading to such decrease in attenuance.

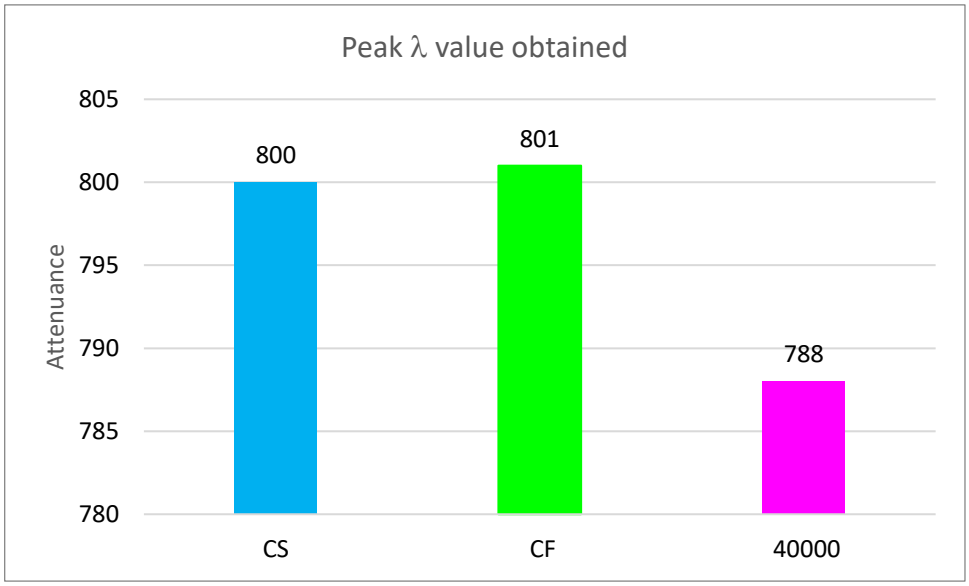

a

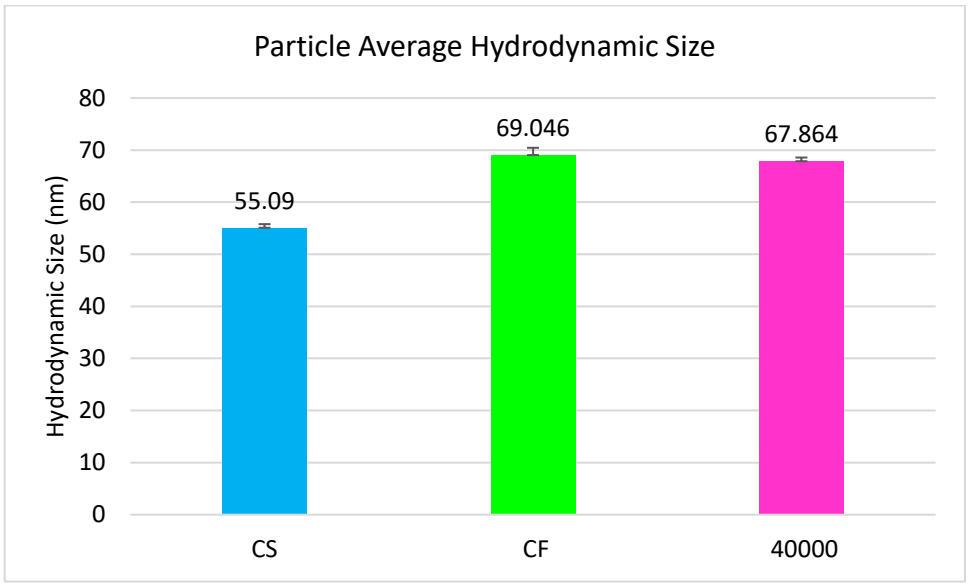

b

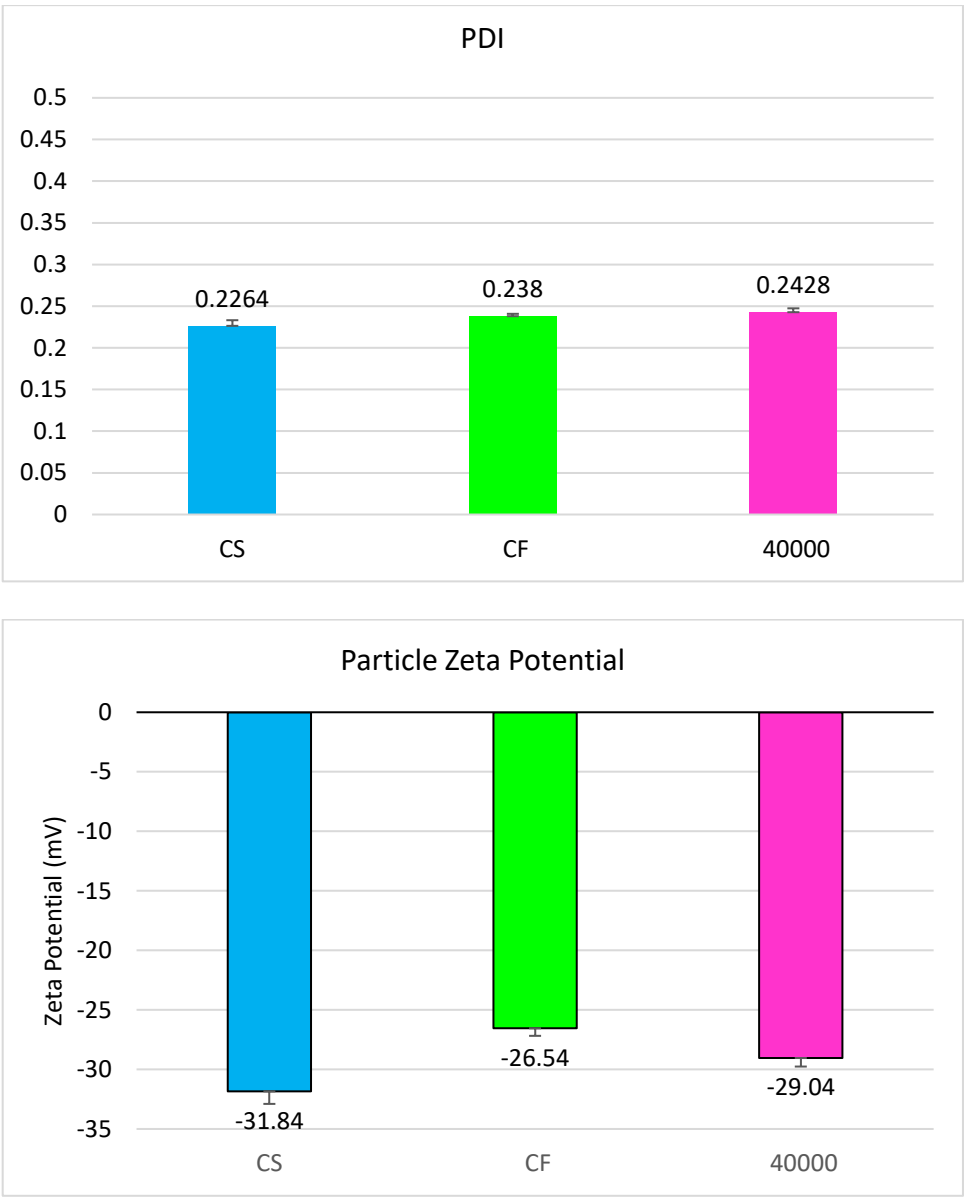

Figure 21 – Visual representation compilation of the results obtained of the selected concentration ratios comparable to the saturation levels verified in the nanospheres previously synthesized, obtained via UV-Vis (10a), DLS (21b and 21c) and ELS (21d).

Also noticeable is the fact that in figure 20, when compared with sample CS, the remainder samples present a lower value of attenuance, however concomitantly the values in figure 21 do not present a possibility of aggregation, as the PDI values are low in 21c and the standard deviation verified in 21b are low. Therefore, the decrease in values are probably due to a loss of material during the protocol.

2.4. Functionalization of PEGylated nanostars via EDC/NHS activation for Gra6II binding – Does shape really matter?

The functionalization of the nanostars was made in the same way as the functionalization of the nanospheres, EDC and NHs were used as linkers for the binding of the Gra6II peptide to the nanostars via incubation.

The method used for both the carbodiimide chemistry and the Gra6II bond to the nanoparticle were reproduced exactly as in chapter “1.3 Functionalization of PEGylated nanospheres via EDC/NHS activation for Gra6II binding – creation of a gold nanoprobe for detection of Toxoplasmosis.”, with the sole exception of the utilization of PEGylated nanostars instead of PEGylated nanospheres. The chemical processes and mechanism are also the same as explained in chapter 1.3.

After the functionalization with the synthetic peptide, one major difference was noted, while the nanospheres maintained their red colour throughout the process, the nanostars after the Gra6II functionalization step presented a colour alteration from blue to transparent, yet no aggregation points were present post-centrifugation. Yet, the sample was analysed via UV-Vis. However, upon analysis the graph did not present any band that was characteristic of nanoparticles of any kind, as seen in figure 22.

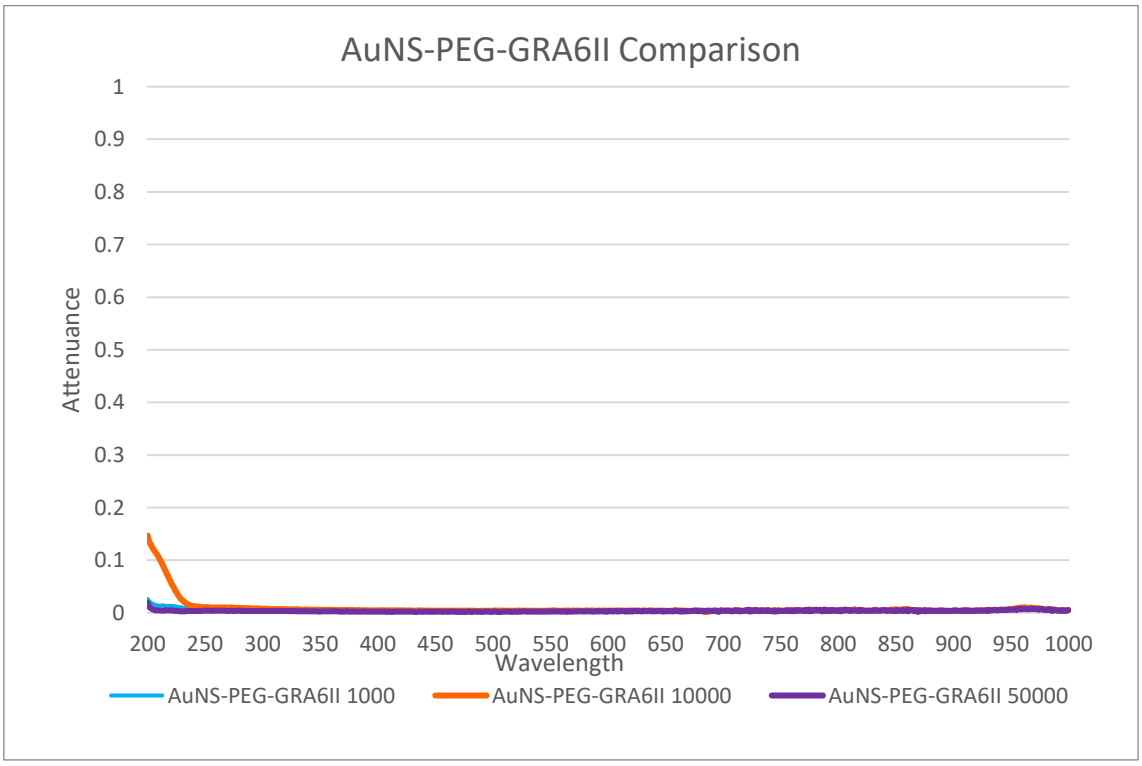

Figure 22 - UV-Vis graph obtained post-UV-Vis spectrophotometry of the different concentrations ratio of the gold nanostars post-Gra6II functionalization. It is possible to verify that no nanoparticles are detected by the UV-Vis spectrophotometer.

However, after characterization via DLS, ELS, as seen in figure 23, and NTA, figure 24, nanoparticles were detected in the transparent medium, however of higher size. As such, it proves that the nanostars did not precipitate after centrifugation and were still present in the samples.

A possibility that the nanostars aggregated into dimers and higher level aggregates during Gra6II incubation, and as such a shift in the emitted light wavelength to energetic levels outside of the one of visible light is not to be excluded.

a

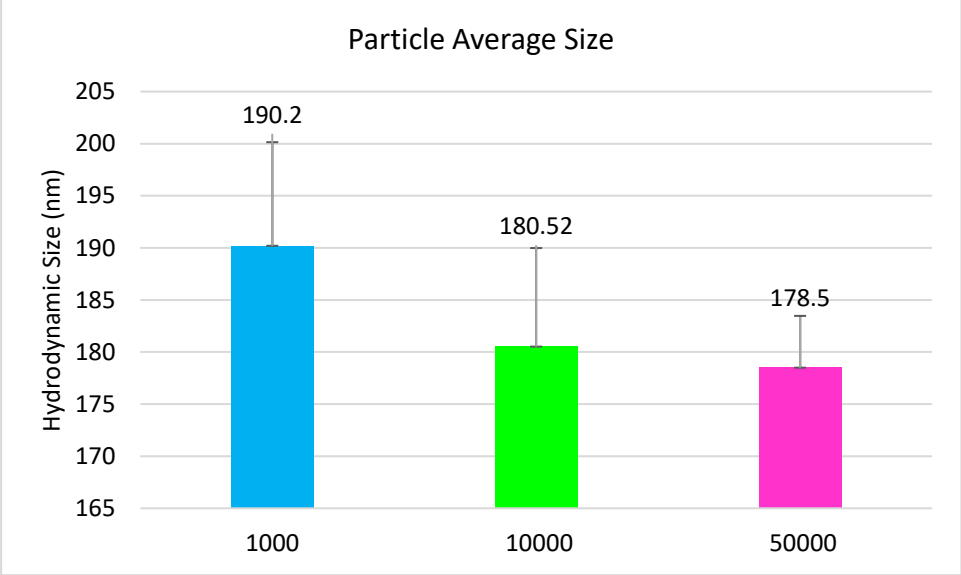

b

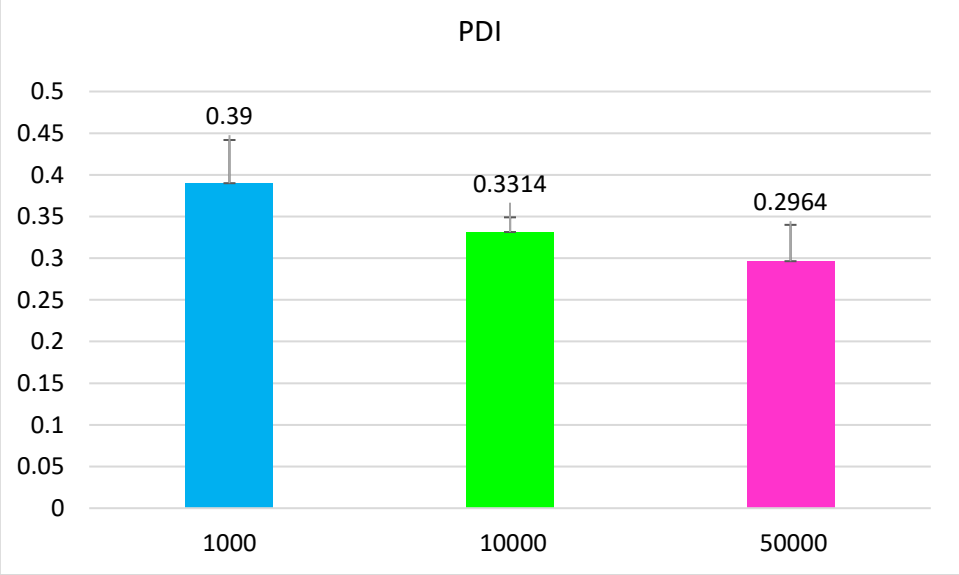

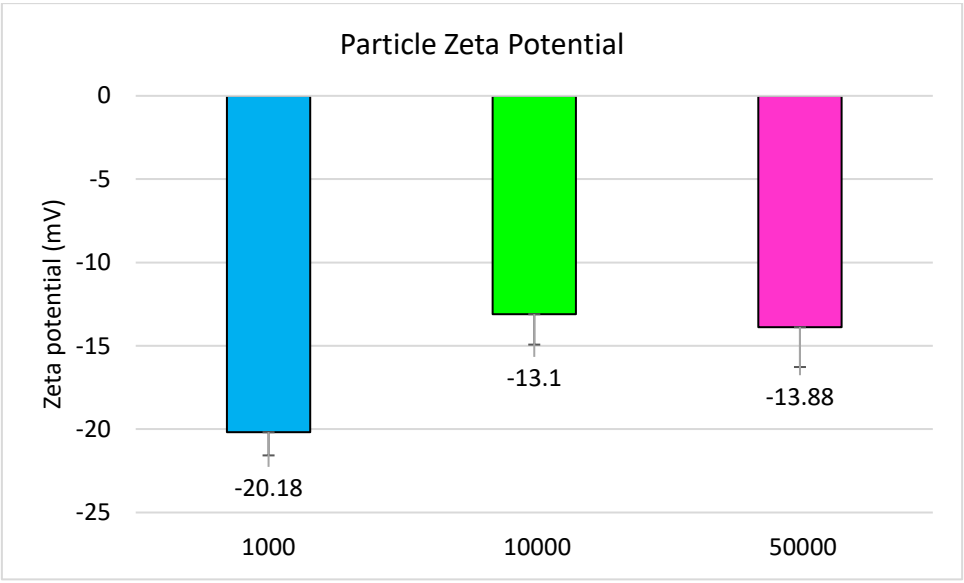

c

Figure 23 – Characterization via DLS (figures 23a and 23b) and ELS (figure 23c). It is noteworthy to see that values present significant differences such as in: a) the values of size are much more higher than before functionalization, which may add to the theory that during the chemical reaction formation of dimer and higher degree of agglomerations has occurred; b) PDI present high values, which goes in concordance with the bars that represent the standard deviation seen in a); c) Zeta potential values show a higher value of alteration than what expected, such being in concordance with the possibility of nanoparticle alteration during chemical reaction during incubation of the synthetic peptide.

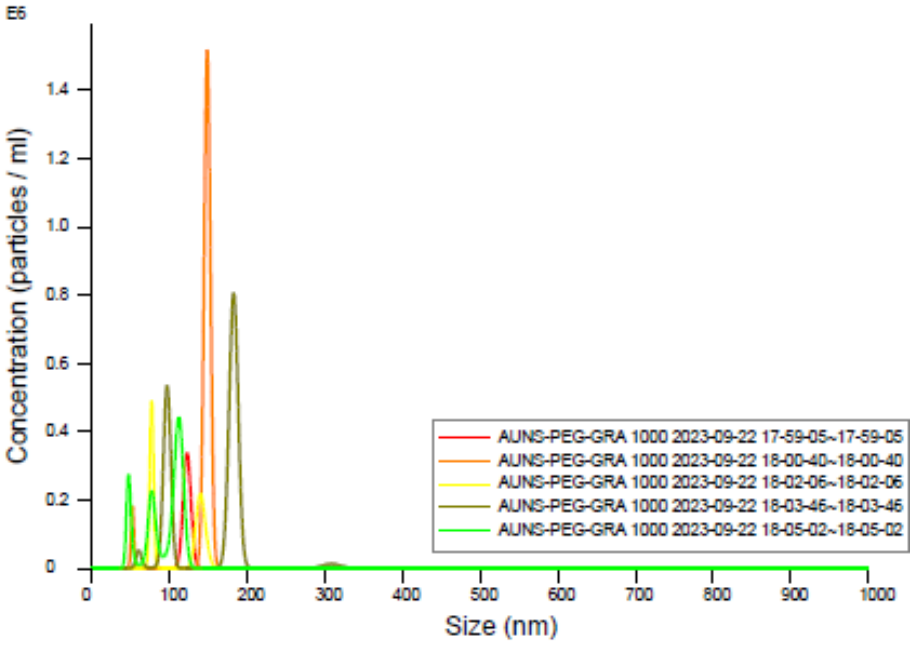

1000

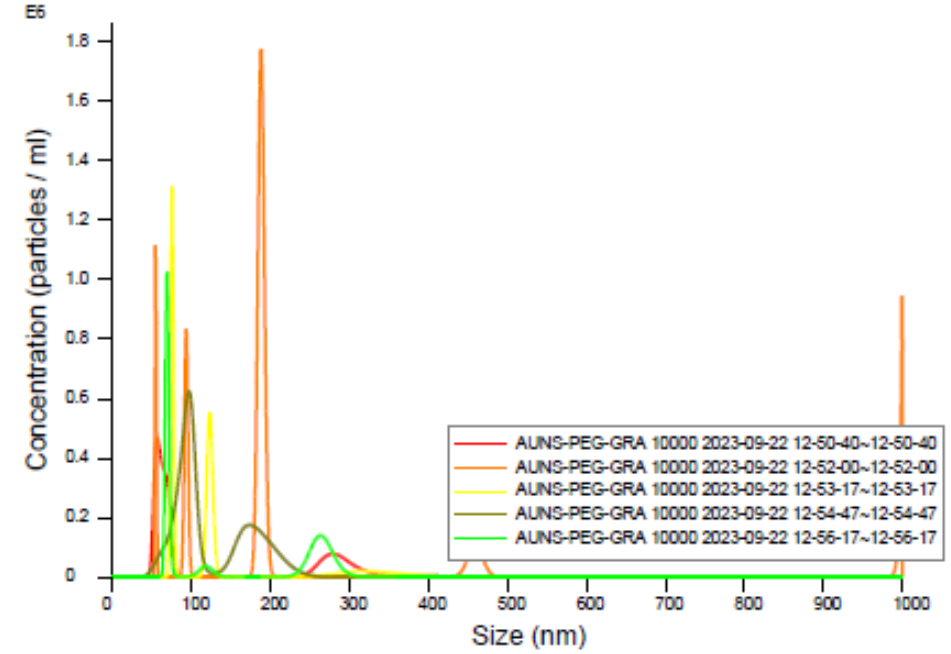

10000

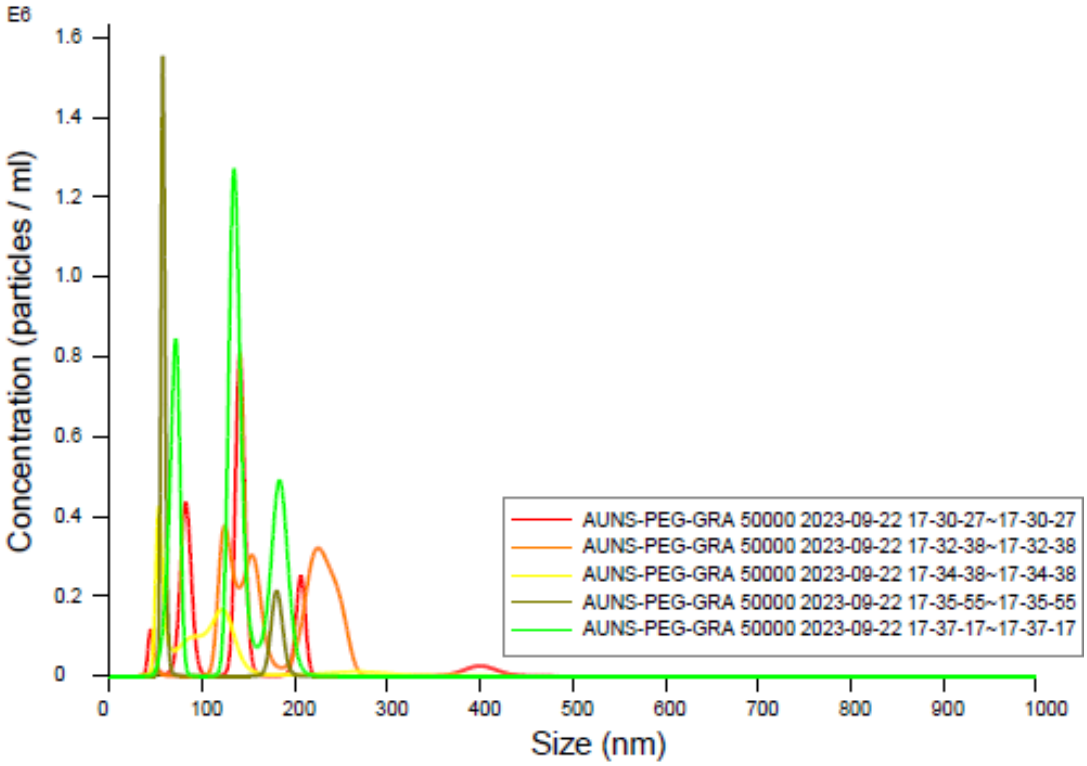

50000

Figure 24 – Characterization of AuS-PEG-Gra6II ratios of Gra6II:AuNS of 1000, 10000 and 50000 via NTA. It is possible to verify in the images that several populations of sizes, each signifying a peak in the graph, exist not only in a high number, but the sizes themselves are of a higher value than what should be expected. Such results also seem to to suggest that aggregation of nanoparticles is present in solution,

Conclusion

Nanospheres presented throughout the functionalization process, from synthesis to Gra6II functionalization, stable values of characterization, chemical stability, and shelf life. Nanosphere synthesis presented itself with good reproducibility, and manipulation of nanospheres for functionalization did not pose any kind of obstacle.

However, nanostars synthesis presented a difficult task due to nanostars being much more sensible to external stimuli. Not only are the ratios amongst reactants and growth agents much more precise than their spherical counterparts, but stimuli such as pH, temperature and other environmental stimuli have to be highly controlled so the synthesis may work. Example of such is temperature, even at room temperature disparities amongst synthesis can be seen, however at lower temperatures the reproducibility amongst synthesis increases. Nanostars also presented a higher sensibility to physical and mechanical stimuli, such as centrifugations, needing lower centrifugations speed due to otherwise presenting a higher possibility of aggregation.

Another important fact to be analysed is the fact that the basis for this test is the visual colorimetric component, where the presence or absence of the target antibodies is characterized by a colour altering aggregation of the nanoprobes. For the nanospheres this condition would prove no problem due to no change in colour during the entire work was noted at a significant level being seen. According to established work [77], the characteristic red colour of nanoparticles when in presence of the target antibodies and salt leads to a change of colour to blue which can be seen in the naked eye, if the test is executed correctly. However, when using the same ratios and concentrations of reactants that were used in nanospheres in this work resulted in already slightly aggregated samples, and the colour of the solution began changing from blue to transparent during Gra6II incubation protocol. This poses as a problem for the development of LFIA sensors, as the colorimetric change of the band without aid of external equipment is necessary. Such would, therefore, also prove a complication for the speed of obtainment of results and the facility of use for non-trained personnel.

Therefore, while theoretically nanostars are presented as a superior option as nanoprobes for the elaboration of SERS based LFIA tests for disease detection when compared to nanospheres, more work should be done to determine what ratios and concentrations to use so that the nanostars could act as nanoprobes in LFIA tests.

´Due to their higher sensitivity when compared to nanospheres, shelf life comparation between tests made utilizing nanospheres as nanoprobes and nanostars as nanoprobes should be made to determine not only which one could be stored for longer periods of time, but also at which conditions storages should be made.

Unfortunately, serological tests were not possible to be executed to test the utilization of the synthesized nanospheres for detection of anti-toxoplasmosis antibodies in serum, due to the lack of infected serum.

In conclusion, while nanostars theoretically present a superior capacity as nanoprobes due to their morphology and signal enhancement capabilities than nanospheres, in practice more work needs to be done to optimize the nanostars as a probe for the elaboration of a LFIA type test immunoassay.

For now, nanospheres present an easier path for the elaboration of such tests and have already presented good potential to be utilized in point of care systems LFIA sensors. Yet, with some work and optimizations to nanostars functionalization protocols, their incorporation in LFIA sensors would be possible, and should not yet be disregarded, for the detection and quantification of anti-toxoplasmosis antibodies, due to their intrinsic signal enhancing characteristics of nanostars.

References

1. Tenter, A.M., A.R. Heckeroth, and L.M. Weiss, *Toxoplasma gondii: from animals to humans.* Int J Parasitol, 2000. **30**(12-13): p. 1217-58.
2. Montoya, J.G. and O. Liesenfeld, *Toxoplasmosis.* Lancet, 2004. **363**(9425): p. 1965-76.
3. Holland, G.N., *Ocular toxoplasmosis: a global reassessment. Part I: epidemiology and course of disease.* Am J Ophthalmol, 2003. **136**(6): p. 973-88.
4. Holland, G.N., *Ocular toxoplasmosis: a global reassessment.* American Journal of Ophthalmology, 2004. **137**(1): p. 1-17.
5. Woodhall D, J.J., Cantey PT, Wilkins PP, Montgomery SP, *Neglected parasitic infections: what every family physician needs to know.* Am Fam Physician., 2014.
6. Dubey, J.P. and J.L. Jones, *Toxoplasma gondii infection in humans and animals in the United States.* Int J Parasitol, 2008. **38**(11): p. 1257-78.
7. Wallon, M. and F. Peyron, *Congenital Toxoplasmosis: A Plea for a Neglected Disease.* Pathogens, 2018. **7**(1).
8. Bigna, J.J., et al., *Global, regional, and country seroprevalence of Toxoplasma gondii in pregnant women: a systematic review, modelling and meta-analysis.* Sci Rep, 2020. **10**(1): p. 12102.
9. Montoya, J.G. and J.S. Remington, *Management of Toxoplasma gondii infection during pregnancy.* Clin Infect Dis, 2008. **47**(4): p. 554-66.
10. Sasai, M. and M. Yamamoto, *Pathogen recognition receptors: ligands and signaling pathways by Toll-like receptors.* Int Rev Immunol, 2013. **32**(2): p. 116-33.
11. Pena, H.F., et al., *Population structure and mouse-virulence of Toxoplasma gondii in Brazil.* Int J Parasitol, 2008. **38**(5): p. 561-9.
12. Rabilloud, M., M. Wallon, and F. Peyron, *In utero and at birth diagnosis of congenital toxoplasmosis: use of likelihood ratios for clinical management.* Pediatr Infect Dis J, 2010. **29**(5): p. 421-5.
13. Wallon, M., et al., *Congenital toxoplasma infection: monthly prenatal screening decreases transmission rate and improves clinical outcome at age 3 years.* Clin Infect Dis, 2013. **56**(9): p. 1223-31.

14. Alves, L.M., et al., *Development of direct assays for Toxoplasma gondii and its use in genomic DNA sample.* J Pharm Biomed Anal, 2017. **145**: p. 838-844.
15. Sousa, S., et al., *Selection of polymorphic peptides from GRA6 and GRA7 sequences of Toxoplasma gondii strains to be used in serotyping.* Clin Vaccine Immunol, 2009. **16**(8): p. 1158-69.
16. Peyron, F., et al., *Serotyping of Toxoplasma gondii in chronically infected pregnant women: predominance of type II in Europe and types I and III in Colombia (South America).* Microbes Infect, 2006. **8**(9-10): p. 2333-40.
17. Kong, J.T., et al., *Serotyping of Toxoplasma gondii infections in humans using synthetic peptides.* J Infect Dis, 2003. **187**(9): p. 1484-95.
18. Sousa, S., et al., *Use of GRA6-derived synthetic polymorphic peptides in an immunoenzymatic assay to serotype Toxoplasma gondii in human serum samples collected from three continents.* Clin Vaccine Immunol, 2008. **15**(9): p. 1380-6.
19. Desmonts, G. and J.S. Remington, *Direct agglutination test for diagnosis of Toxoplasma infection: method for increasing sensitivity and specificity.* J Clin Microbiol, 1980. **11**(6): p. 562-8.
20. Robert-Gangneux, F. and M.L. Darde, *Epidemiology of and diagnostic strategies for toxoplasmosis.* Clin Microbiol Rev, 2012. **25**(2): p. 264-96.
21. Sue, M.J., et al., *Application of PCR-ELISA in molecular diagnosis.* Biomed Res Int, 2014. **2014**: p. 653014.
22. Iha, K., et al., *Ultrasensitive ELISA Developed for Diagnosis.* Diagnostics (Basel), 2019. **9**(3).
23. Tsurusawa, N., et al., *Modified ELISA for Ultrasensitive Diagnosis.* J Clin Med, 2021. **10**(21).
24. Hedman, K., et al., *Recent primary toxoplasma infection indicated by a low avidity of specific IgG.* J Infect Dis, 1989. **159**(4): p. 736-40.
25. Teimouri, A., et al., *Role of Toxoplasma gondii IgG Avidity Testing in Discriminating between Acute and Chronic Toxoplasmosis in Pregnancy.* J Clin Microbiol, 2020. **58**(9).
26. Holliman, R.E., et al., *The diagnosis of toxoplasmosis using IgG avidity.* Epidemiol Infect, 1994. **112**(2): p. 399-408.
27. Araujo, P.R. and A.W. Ferreira, *Avidity of IgG antibodies against excreted/secreted antigens of Toxoplasma gondii: immunological marker for acute recent toxoplasmosis.* Rev Soc Bras Med Trop, 2008. **41**(2): p. 142-7.

28. Sasai, M., A. Pradipta, and M. Yamamoto, *Host immune responses to Toxoplasma gondii.* Int Immunol, 2018. **30**(3): p. 113-119.
29. *WHO Meeting of Investigators on Toxoplasmosis (1968: Geneva, Switzerland) & World Health Organization. (1969). Toxoplasmosis : report of a WHO meeting of investigators [meeting held in Geneva from 25 to 29 November 1968]. World Health Organization.*
30. *Congenital toxoplasmosis Annual Epidemiological Report for 2019.*
31. *European Centre for Disease Prevention and Control. Congenital toxoplasmosis. In: ECDC. Annual epidemiological report for 2019. Stockholm: ECDC; 2022.*
32. Tan, S.Y. and S. Grimes, *Paul Ehrlich (1854-1915): man with the magic bullet.* Singapore Med J, 2010. **51**(11): p. 842-3.
33. Winau, F., O. Westphal, and R. Winau, *Paul Ehrlich--in search of the magic bullet.* Microbes Infect, 2004. **6**(8): p. 786-9.
34. Alyautdin, R., *A Brief History of Progress on Nanotechnology: When Will the 'Magic' Nanobullet Shoot?* Journal of Clinical and Health Sciences, 2018. **3**(1).
35. Anu Mary Ealia, S. and M.P. Saravanakumar, *A review on the classification, characterisation, synthesis of nanoparticles and their application.* IOP Conference Series: Materials Science and Engineering, 2017. **263**.
36. Baptista, P., et al., *Gold nanoparticles for the development of clinical diagnosis methods.* Anal Bioanal Chem, 2008. **391**(3): p. 943-50.
37. Andreiuk, B., et al., *Design and synthesis of gold nanostars-based SERS nanotags for bioimaging applications.* Nanotheranostics, 2022. **6**(1): p. 10-30.
38. Begeman, I.J., et al., *Point-of-care testing for Toxoplasma gondii IgG/IgM using Toxoplasma ICT IgG-IgM test with sera from the United States and implications for developing countries.* PLoS Negl Trop Dis, 2017. **11**(6): p. e0005670.
39. Cavadas, M.A.S., et al., *Unravelling Malaria Antigen Binding to Antibody-Gold Nanoparticle Conjugates.* Particle & Particle Systems Characterization, 2016. **33**(12): p. 906-915.
40. Chapey, E., M. Wallon, and F. Peyron, *Evaluation of the LDBIO point of care test for the combined detection of toxoplasmic IgG and IgM.* Clin Chim Acta, 2017. **464**: p. 200-201.
41. de Almeida, M.P., et al., *Silver Nanostar-Based SERS for the Discrimination of Clinically Relevant Acinetobacter baumannii and Klebsiella pneumoniae Species and Clones.* Biosensors (Basel), 2023. **13**(2).

42. Eaton, P., et al., *Imaging gold nanoparticles for DNA sequence recognition in biomedical applications.* IEEE Trans Nanobioscience, 2007. **6**(4): p. 282-8.
43. Jazayeri, M.H., et al., *Various methods of gold nanoparticles (GNPs) conjugation to antibodies.* Sensing and Bio-Sensing Research, 2016. **9**: p. 17-22.
44. Raghav, R. and S. Srivastava, *Immobilization strategy for enhancing sensitivity of immunosensors: L-Asparagine-AuNPs as a promising alternative of EDC-NHS activated citrate-AuNPs for antibody immobilization.* Biosens Bioelectron, 2016. **78**: p. 396-403.
45. Zhang, Q., et al., *Study of Efficiency of Coupling Peptides with Gold Nanoparticles.* Chinese Journal of Analytical Chemistry, 2017. **45**(5): p. 662-667.
46. Smita, S., et al., *Nanoparticles in the environment: assessment using the causal diagram approach.* Environ Health, 2012. **11 Suppl 1**(Suppl 1): p. S13.
47. *Tiwari, Dhermendra & Behari, J. & Sen, Prasenjit. (2008). Application of Nanoparticles in Waste Water Treatment. World Applied Sciences Journal. 3. .*
48. Salavati-Niasari, M., F. Davar, and N. Mir, *Synthesis and characterization of metallic copper nanoparticles via thermal decomposition.* Polyhedron, 2008. **27**(17): p. 3514-3518.
49. Tai, C.Y., et al., *Synthesis of Magnesium Hydroxide and Oxide Nanoparticles Using a Spinning Disk Reactor.* Industrial & Engineering Chemistry Research, 2007. **46**(17): p. 5536-5541.
50. Bhaviripudi, S., et al., *CVD synthesis of single-walled carbon nanotubes from gold nanoparticle catalysts.* J Am Chem Soc, 2007. **129**(6): p. 1516-7.
51. Prasad Yadav, T., R. Manohar Yadav, and D. Pratap Singh, *Mechanical Milling: a Top Down Approach for the Synthesis of Nanomaterials and Nanocomposites.* Nanoscience and Nanotechnology, 2012. **2**(3): p. 22-48.
52. Pimpin, A. and W. Srituravanich, *Review on Micro- and Nanolithography Techniques and their Applications.* Engineering Journal, 2012. **16**(1): p. 37-56.
53. Ramesh, S., *Sol-Gel Synthesis and Characterization of Nanoparticles.* Journal of Nanoscience, 2013. **2013**: p. 1-8.
54. Mohammadi, S., A. Harvey, and K.V.K. Boodhoo, *Synthesis of TiO2 nanoparticles in a spinning disc reactor.* Chemical Engineering Journal, 2014. **258**: p. 171-184.

55. Haynes, C.L. and R.P. Van Duyne, *Nanosphere Lithography: A Versatile Nanofabrication Tool for Studies of Size-Dependent Nanoparticle Optics.* The Journal of Physical Chemistry B, 2001. **105**(24): p. 5599-5611.
56. Shah, P. and A. Gavrin, *Synthesis of nanoparticles using high-pressure sputtering for magnetic domain imaging.* Journal of Magnetism and Magnetic Materials, 2006. **301**(1): p. 118-123.
57. Lugscheider, E., et al., *Magnetron-sputtered hard material coatings on thermoplastic polymers for clean room applications.* Surface and Coatings Technology, 1998. **108-109**: p. 398-402.
58. Amendola, V. and M. Meneghetti, *Laser ablation synthesis in solution and size manipulation of noble metal nanoparticles.* Phys Chem Chem Phys, 2009. **11**(20): p. 3805-21.
59. Kammler, H.K., L. Mädler, and S.E. Pratsinis, *Flame Synthesis of Nanoparticles.* Chemie Ingenieur Technik, 2001. **73**: p. 708-708.
60. D'Amato, R., et al., *Synthesis of ceramic nanoparticles by laser pyrolysis: From research to applications.* Journal of Analytical and Applied Pyrolysis, 2013. **104**: p. 461-469.
61. Kuppusamy, P., et al., *Biosynthesis of metallic nanoparticles using plant derivatives and their new avenues in pharmacological applications - An updated report.* Saudi Pharm J, 2016. **24**(4): p. 473-84.
62. Carter, J.D. and T.H. Labean, *Coupling strategies for the synthesis of Peptide-oligonucleotide conjugates for patterned synthetic biomineralization.* J Nucleic Acids, 2011. **2011**: p. 926595.
63. Pramanik, A., et al., *Aptamer Conjugated Gold Nanostar-Based Distance-Dependent Nanoparticle Surface Energy Transfer Spectroscopy for Ultrasensitive Detection and Inactivation of Corona Virus.* J Phys Chem Lett, 2021. **12**(8): p. 2166-2171.
64. Kreuter, J., *Nanoparticles--a historical perspective.* Int J Pharm, 2007. **331**(1): p. 1-10.
65. Rahme, K., et al., *PEGylated gold nanoparticles: polymer quantification as a function of PEG lengths and nanoparticle dimensions.* RSC Adv., 2013. **3**(17): p. 6085-6094.
66. Tlotleng, N., et al., *Cytotoxicity, intracellular localization and exocytosis of citrate capped and PEG functionalized gold nanoparticles in human hepatocyte and kidney cells.* Cell Biol Toxicol, 2016. **32**(4): p. 305-21.

67. Yuan, H., A.M. Fales, and T. Vo-Dinh, *TAT peptide-functionalized gold nanostars: enhanced intracellular delivery and efficient NIR photothermal therapy using ultralow irradiance.* J Am Chem Soc, 2012. **134**(28): p. 11358-61.
68. Bocca, C., et al., *Phagocytic uptake of fluorescent stealth and non-stealth solid lipid nanoparticles.* International Journal of Pharmaceutics, 1998. **175**(2): p. 185-193.
69. Zara, G.P., et al., *Intravenous administration to rabbits of non-stealth and stealth doxorubicin-loaded solid lipid nanoparticles at increasing concentrations of stealth agent: pharmacokinetics and distribution of doxorubicin in brain and other tissues.* J Drug Target, 2002. **10**(4): p. 327-35.
70. Zalba S, T.H.T., Burgui C, Garrido MJ. Stealth nanoparticles in oncology: Facing the PEG dilemma. J Control Release. 2022 Nov;351:22-36. doi: 10.1016/j.jconrel.2022.09.002. Epub 2022 Sep 19. PMID: 36087801.
71. Amoozgar, Z. and Y. Yeo, *Recent advances in stealth coating of nanoparticle drug delivery systems.* Wiley Interdiscip Rev Nanomed Nanobiotechnol, 2012. **4**(2): p. 219-33.
72. Zamboni, W.C., *Liposomal, nanoparticle, and conjugated formulations of anticancer agents.* Clin Cancer Res, 2005. **11**(23): p. 8230-4.
73. Cheng, L., et al., *Organic stealth nanoparticles for highly effective in vivo near-infrared photothermal therapy of cancer.* ACS Nano, 2012. **6**(6): p. 5605-13.
74. Schutz, M., et al., *Hydrophilically stabilized gold nanostars as SERS labels for tissue imaging of the tumor suppressor p63 by immuno-SERS microscopy.* Chem Commun (Camb), 2011. **47**(14): p. 4216-8.
75. Stanković, V., et al., *Anti-human albumin monoclonal antibody immobilized on EDC-NHS functionalized carboxylic graphene/AuNPs composite as promising electrochemical HSA immunosensor.* Journal of Electroanalytical Chemistry, 2020. **860**.
76. Bartczak, D. and A.G. Kanaras, *Preparation of peptide-functionalized gold nanoparticles using one pot EDC/sulfo-NHS coupling.* Langmuir, 2011. **27**(16): p. 10119-23.
77. Sousa, S., et al., *Biosensor Based Immunoassay: A New Approach for Serotyping of Toxoplasma gondii.* Nanomaterials (Basel), 2021. **11**(8).
78. Zong, J., S.L. Cobb, and N.R. Cameron, *Peptide-functionalized gold nanoparticles: versatile biomaterials for diagnostic and therapeutic applications.* Biomater Sci, 2017. **5**(5): p. 872-886.

79. Lecordier, L., et al., *Characterization of a dense granule antigen of Toxoplasma gondii (GRA6) associated to the network of the parasitophorous vacuole.* Mol Biochem Parasitol, 1995. **70**(1-2): p. 85-94.
80. Gatkowska, J., et al., *Toxoplasma gondii: an evaluation of diagnostic value of recombinant antigens in a murine model.* Exp Parasitol, 2006. **114**(3): p. 220-7.
81. Golkar, M., et al., *Serodiagnosis of recently acquired Toxoplasma gondii infection in pregnant women using enzyme-linked immunosorbent assays with a recombinant dense granule GRA6 protein.* Diagn Microbiol Infect Dis, 2008. **61**(1): p. 31-9.
82. Redlich, A. and W.A. Muller, *Serodiagnosis of acute toxoplasmosis using a recombinant form of the dense granule antigen GRA6 in an enzyme-linked immunosorbent assay.* Parasitol Res, 1998. **84**(9): p. 700-6.
83. Akbar, R., et al., *A compact vocabulary of paratope-epitope interactions enables predictability of antibody-antigen binding.* Cell Rep, 2021. **34**(11): p. 108856.
84. Aalberse, R.C. and R. Crameri, *IgE-binding epitopes: a reappraisal.* Allergy, 2011. **66**(10): p. 1261-74.
85. Van Regenmortel, M.H., *The concept and operational definition of protein epitopes.* Philos Trans R Soc Lond B Biol Sci, 1989. **323**(1217): p. 451-66.
86. Van Oss, C.J., *Hydrophobic, hydrophilic and other interactions in epitope-paratope binding.* Mol Immunol, 1995. **32**(3): p. 199-211.
87. Balasubramanian, S.K., et al., *Characterization, purification, and stability of gold nanoparticles.* Biomaterials, 2010. **31**(34): p. 9023-30.
88. Barbosa, S., et al., *Tuning size and sensing properties in colloidal gold nanostars.* Langmuir, 2010. **26**(18): p. 14943-50.
89. Becerril-Castro, I.B., et al., *Gold Nanostars: Synthesis, Optical and SERS Analytical Properties.* Analysis & Sensing, 2022. **2**(3).
90. Dallari, C., et al., *Gold Nanostars Bioconjugation for Selective Targeting and SERS Detection of Biofluids.* Nanomaterials (Basel), 2021. **11**(3).
91. Fabris, L., *Gold Nanostars in Biology and Medicine: Understanding Physicochemical Properties to Broaden Applicability.* The Journal of Physical Chemistry C, 2020. **124**(49): p. 26540-26553.
92. Hao, F., et al., *Plasmon resonances of a gold nanostar.* Nano Lett, 2007. **7**(3): p. 729-32.

93. Khoury, C.G. and T. Vo-Dinh, *Gold Nanostars For Surface-Enhanced Raman Scattering: Synthesis, Characterization and Optimization.* J Phys Chem C Nanomater Interfaces, 2008. **2008**(112): p. 18849-18859.
94. Lu, G., T.Z. Forbes, and A.J. Haes, *SERS detection of uranyl using functionalized gold nanostars promoted by nanoparticle shape and size.* Analyst, 2016. **141**(17): p. 5137-43.
95. Pallavicini, P., E. Cabrini, and M. Borzenkov, *Gold Nanostar Synthesis and Functionalization with Organic Molecules*, in *Gold Nanostars*. 2015. p. 1-23.
96. Dardir, K., et al., *SERS Nanoprobe for Intracellular Monitoring of Viral Mutations.* The Journal of Physical Chemistry C, 2020. **124**(5): p. 3211-3217.
97. Donoso-Gonzalez, O., et al., *Functionalization of Gold Nanostars with Cationic beta-Cyclodextrin-Based Polymer for Drug Co-Loading and SERS Monitoring.* Pharmaceutics, 2021. **13**(2).
98. OLIVEIRA, M.J.Q.D., *NANOSERS MICROFLUIDICS PLATFORM FOR RAPID SCREENING FOR INFECTIOUS DISEASES*.
99. Senthil Kumar, P., et al., *High-yield synthesis and optical response of gold nanostars.* Nanotechnology, 2008. **19**(1): p. 015606.
100. Su, Q., et al., *A reproducible SERS substrate based on electrostatically assisted APTES-functionalized surface-assembly of gold nanostars.* ACS Appl Mater Interfaces, 2011. **3**(6): p. 1873-9.
101. GenÇ, O., et al., *Development and validation of sandwich quantitative ELISA prototypebased on the bovine IFNg for the detection of cellular immunity.* Turkish Journal of Veterinary and Animal Sciences, 2015. **39**: p. 724-729.
102. Zhang, Y., et al., *Development of a double monoclonal antibody-based sandwich enzyme-linked immunosorbent assay for detecting canine distemper virus.* Appl Microbiol Biotechnol, 2020. **104**(24): p. 10725-10735.
103. Van Maanen, C. and C. Terpstra, *Comparison of a liquid-phase blocking sandwich ELISA and a serum neutralization test to evaluate immunity in potency tests of foot-and-mouth disease vaccines.* J Immunol Methods, 1989. **124**(1): p. 111-9.
104. Periolo, O.H., et al., *Large-scale use of liquid-phase blocking sandwich ELISA for the evaluation of protective immunity against aphthovirus in cattle vaccinated with oil-adjuvanted vaccines in Argentina.* Vaccine, 1993. **11**(7): p. 754-60.

105. Wang, C., D. Liu, and Z. Wang, *Gold nanoparticle based dot-blot immunoassay for sensitively detecting Alzheimer's disease related beta-amyloid peptide.* Chem Commun (Camb), 2012. **48**(67): p. 8392-4.
106. Dykman, L.A., *Gold nanoparticles for preparation of antibodies and vaccines against infectious diseases.* Expert Rev Vaccines, 2020. **19**(5): p. 465-477.
107. Guo, Y.Y., et al., *Strategies for Precise Engineering and Conjugation of Antibody Targeted-nanoparticles for Cancer Therapy.* Curr Med Sci, 2020. **40**(3): p. 463-473.
108. Cardenas, M., et al., *Thiol-specific and nonspecific interactions between DNA and gold nanoparticles.* Langmuir, 2006. **22**(7): p. 3294-9.
109. Oliveira, M.J., et al., *Design and Simple Assembly of Gold Nanostar Bioconjugates for Surface-Enhanced Raman Spectroscopy Immunoassays.* Nanomaterials (Basel), 2019. **9**(11).
110. Schlucker, S., *Surface-enhanced Raman spectroscopy: concepts and chemical applications.* Angew Chem Int Ed Engl, 2014. **53**(19): p. 4756-95.
111. Giannini, V., R. Rodríguez-Oliveros, and J.A. Sánchez-Gil, *Surface Plasmon Resonances of Metallic Nanostars/Nanoflowers for Surface-Enhanced Raman Scattering.* Plasmonics, 2010. **5**(1): p. 99-104.
112. Ma, W.Y., et al., *A numerical investigation of the effect of vertex geometry on localized surface plasmon resonance of nanostructures.* Opt Express, 2010. **18**(2): p. 843-53.
113. Nehl, C.L., H. Liao, and J.H. Hafner, *Optical properties of star-shaped gold nanoparticles.* Nano Lett, 2006. **6**(4): p. 683-8.
114. Oliveira, M.J., et al., *Office paper decorated with silver nanostars - an alternative cost effective platform for trace analyte detection by SERS.* Sci Rep, 2017. **7**(1): p. 2480.
115. Wang, L., et al., *SERS-based test strips: Principles, designs and applications.* Biosens Bioelectron, 2021. **189**: p. 113360.
116. Shan, B., et al., *Novel SERS labels: Rational design, functional integration and biomedical applications.* Coordination Chemistry Reviews, 2018. **371**: p. 11-37.
117. Hwang, J., S. Lee, and J. Choo, *Application of a SERS-based lateral flow immunoassay strip for the rapid and sensitive detection of staphylococcal enterotoxin B.* Nanoscale, 2016. **8**(22): p. 11418-25.
118. Guo, J., et al., *Preparation and application of microfluidic SERS substrate: Challenges and future perspectives.* Journal of Materials Science & Technology, 2020. **37**: p. 96-103.

119. Posthuma-Trumpie, G.A., J. Korf, and A. van Amerongen, *Lateral flow (immuno)assay: its strengths, weaknesses, opportunities and threats. A literature survey.* Anal Bioanal Chem, 2009. **393**(2): p. 569-82.
120. Parolo, C., A. de la Escosura-Muniz, and A. Merkoci, *Enhanced lateral flow immunoassay using gold nanoparticles loaded with enzymes.* Biosens Bioelectron, 2013. **40**(1): p. 412-6.
121. .
122. Moyano, A., et al., *Magnetic Lateral Flow Immunoassays.* Diagnostics (Basel), 2020. **10**(5).
123. Chen, Y., et al., *A Ligand System for the Flexible Functionalization of Quantum Dots via Click Chemistry.* Angew Chem Int Ed Engl, 2018. **57**(17): p. 4652-4656.
124. Liesenfeld, O., et al., *Effect of testing for IgG avidity in the diagnosis of Toxoplasma gondii infection in pregnant women: experience in a US reference laboratory.* J Infect Dis, 2001. **183**(8): p. 1248-53.
125. *Bretherick's Handbook of Reactive Chemical Hazards*. Bretherick's Handbook of Reactive Chemical Hazards ed. Vol. Volume 2. 1999, Linacre House, Jordan Hill, Oxford OX2 8DP: Butterworth-Heinemann Ltd.
126. Zabetakis, K., et al., *Effect of high gold salt concentrations on the size and polydispersity of gold nanoparticles prepared by an extended Turkevich–Frens method.* Gold Bulletin, 2012. **45**(4): p. 203-211.
127. Kimling, J., et al., *Turkevich method for gold nanoparticle synthesis revisited.* J Phys Chem B, 2006. **110**(32): p. 15700-7.
128. Dong, J., et al., *Synthesis of Precision Gold Nanoparticles Using Turkevich Method.* Kona, 2020. **37**: p. 224-232.
129. Haiss, W., et al., *Determination of size and concentration of gold nanoparticles from UV-vis spectra.* Anal Chem, 2007. **79**(11): p. 4215-21.
130. Turkevich, J., P.C. Stevenson, and J. Hillier, *A study of the nucleation and growth processes in the synthesis of colloidal gold.* Discussions of the Faraday Society, 1951. **11**.
131. Frens, G., *Particle size and sol stability in metal colloids.* Kolloid-Zeitschrift und Zeitschrift für Polymere, 1972. **250**(7): p. 736-741.
132. Frens, G., *Controlled Nucleation for the Regulation of the Particle Size in Monodisperse Gold Suspensions.* Nature Physical Science, 1973. **241**(105): p. 20-22.

133. Ji, X., et al., *Size control of gold nanocrystals in citrate reduction: the third role of citrate.* J Am Chem Soc, 2007. **129**(45): p. 13939-48.
134. Zhao, P., N. Li, and D. Astruc, *State of the art in gold nanoparticle synthesis.* Coordination Chemistry Reviews, 2013. **257**(3-4): p. 638-665.
135. Yuan, H., et al., *Gold nanostars: surfactant-free synthesis, 3D modelling, and two-photon photoluminescence imaging.* Nanotechnology, 2012. **23**(7): p. 075102.
136. Menéndez-Manjón, A. and S. Barcikowski, *Hydrodynamic size distribution of gold nanoparticles controlled by repetition rate during pulsed laser ablation in water.* Applied Surface Science, 2011. **257**(9): p. 4285-4290.
137. Zheng, T., et al., *A simple and fast method to study the hydrodynamic size difference of protein disulfide isomerase in oxidized and reduced form using gold nanoparticles and dynamic light scattering.* Analyst, 2016. **141**(3): p. 934-8.
138. Takagi, T., *Electrophoretic light scattering.* Electrophoresis, 1993. **14**(12): p. 1255-6.
139. (2002). Electrophoretic Light Scattering. In: Scarlett, B.e.P.C.L.S.M.P.T.S., vol 13. Springer, Dordrecht..
140. Thambiliyagodage, C., *Ligand exchange reactions and PEG stabilization of gold nanoparticles.* Current Research in Green and Sustainable Chemistry, 2022. **5**.
141. Que, Y., et al., *Stability and Catalytic Activity of PEG-b-PS-Capped Gold Nanoparticles: A Matter of PS Chain Length.* The Journal of Physical Chemistry C, 2015. **119**(4): p. 1960-1970.
142. Larson-Smith, K. and D.C. Pozzo, *Competitive adsorption of thiolated poly(ethylene glycol) and alkane-thiols on gold nanoparticles and its effect on cluster formation.* Langmuir, 2012. **28**(37): p. 13157-65.
143. Jadzinsky, P.D., et al., *Structure of a thiol monolayer-protected gold nanoparticle at 1.1 A resolution.* Science, 2007. **318**(5849): p. 430-3.
144. Larsson, J.A., M. Nolan, and J.C. Greer, *Interactions between Thiol Molecular Linkers and the Au13 Nanoparticle.* The Journal of Physical Chemistry B, 2002. **106**(23): p. 5931-5937.
145. Xue, Y., et al., *Quantifying thiol-gold interactions towards the efficient strength control.* Nat Commun, 2014. **5**: p. 4348.
146. Zanchet, D., et al., *Inter-atomic distance contraction in thiol-passivated gold nanoparticles.* Chemical Physics Letters, 2000. **323**(1-2): p. 167-172.
147. Sousa, S., et al., *Serotyping Toxoplasma Gondii: A Cross-Sectional Study in Uruguay.* Journal of Infectious Diseases and Epidemiology, 2017. **3**(3).

148. dilemma, S.n.i.o.F.t.P., *Sara Zalba, Timo L.M. ten Hagen, Carmen Burgui, María J. Garrido,.* Journal of Controlled Release.
149. Keleştemur, S., M. Altunbek, and M. Culha, *Influence of EDC/NHS coupling chemistry on stability and cytotoxicity of ZnO nanoparticles modified with proteins.* Applied Surface Science, 2017. **403**: p. 455-463.
150. Li, D., et al., *Immobilization of glucose oxidase onto gold nanoparticles with enhanced thermostability.* Biochem Biophys Res Commun, 2007. **355**(2): p. 488-93.
151. Park, C., et al., *New method and characterization of self-assembled gelatin-oleic nanoparticles using a desolvation method via carbodiimide/N-hydroxysuccinimide (EDC/NHS) reaction.* Eur J Pharm Biopharm, 2015. **89**: p. 365-73.
152. Hammond, J.L., et al., *Localized surface plasmon resonance as a biosensing platform for developing countries.* Biosensors (Basel), 2014. **4**(2): p. 172-88.
153. Sriram, M., et al., *Single nanoparticle plasmonic sensors.* Sensors (Basel), 2015. **15**(10): p. 25774-92.
154. Moskovits, M., *Surface-enhanced spectroscopy.* Reviews of Modern Physics, 1985. **57**(3): p. 783-826.
155. Guerrero-Martínez, A., et al., *Nanostars shine bright for you.* Current Opinion in Colloid & Interface Science, 2011. **16**(2): p. 118-127.
156. Liz-Marzan, L.M., *Tailoring surface plasmons through the morphology and assembly of metal nanoparticles.* Langmuir, 2006. **22**(1): p. 32-41.
157. Alvarez-Puebla, R., L.M. Liz-Marzán, and F.J. García de Abajo, *Light Concentration at the Nanometer Scale.* The Journal of Physical Chemistry Letters, 2010. **1**(16): p. 2428-2434.
158. Nikoobakht, B. and M.A. El-Sayed, *Preparation and Growth Mechanism of Gold Nanorods (NRs) Using Seed-Mediated Growth Method.* Chemistry of Materials, 2003. **15**(10): p. 1957-1962.
159. Brus, L., *Noble metal nanocrystals: plasmon electron transfer photochemistry and single-molecule Raman spectroscopy.* Acc Chem Res, 2008. **41**(12): p. 1742-9.
160. Rodríguez-Lorenzo, L., et al., *Surface Enhanced Raman Scattering Using Star-Shaped Gold Colloidal Nanoparticles.* The Journal of Physical Chemistry C, 2009. **114**(16): p. 7336-7340.

161. Xu, H., et al., *Spectroscopy of Single Hemoglobin Molecules by Surface Enhanced Raman Scattering.* Physical Review Letters, 1999. **83**(21): p. 4357-4360.

162. Depciuch, J., et al., *Control of Arms of Au Stars Size and its Dependent Cytotoxicity and Photosensitizer Effects in Photothermal Anticancer Therapy.* Int J Mol Sci, 2019. **20**(20).